TEXAS INSTRUMENTS
INCORPORATED

HEAT STERILIZABLE AND IMPACT RESISTANT Ni-Cd BATTERY DEVELOPMENT

Jet Propulsion Laboratory

Contract No. 951972, Modification No. 6

Report for Eighth Quarter
April 1 to June 30, 1969

by

P.V. Popat: Project Manager
Principal Contributors:
R.L. Crawford: Electrochemistry
J.M. Gondusky: Impact Resistant Cells
E.J. Rubin: Battery Engineering

TEXAS INSTRUMENTS INCORPORATED
Research and Development Laboratories
Attleboro, Massachusetts

This work was performed for the Jet Propulsion Laboratory, California Institute of Technology, sponsored by the National Aeronautics and Space Administration under Contract NAS-7-100; Task Order No. RD-26.

metallurgical
materials division

I N D E X

NOTICE

This report was prepared as an account of government-sponsored work. Neither the United States, nor the National Aeronautics and Space Administration (NASA), nor any person acting on behalf of NASA:

(a) makes warranty of representation, expressed or implied with respect to the accuracy, completeness, or usefulness of the information contained in this report, or that the use of any information, apparatus, method, or process disclosed in this report may not infringe privately owned rights;

(b) assumes any liabilities with respect to the use of, or for damages resulting from the use of any information, apparatus, method or process disclosed in this report.

As used above, "person acting on behalf of NASA" includes any employees or contractor of NASA, or employee of such contractor to the extent that such contractor, prepares, disseminates, or provides access to any information pursuant to his employment with such contractor.

Request for copies of this report should be referred to:

National Aeronautics and Space Administration
Office of Scientific and Technical Information
Attention: AFSS-A

ABSTRACT

I. Development of Heat-Sterilizable Ni-Cd Cells:
Since the engineering capability of satisfactory heat-sterilizable cells has been proven as demonstrated by extensive post-sterilization cycling at 100% d.o.d. of sealed 4AH and 25AH prismatic and 25AH cylindrical cells without significant performance change, further electrochemical investigations were directed towards better understanding of the behavior of sterilized positive and negative electrodes. Emphasis was placed on open circuit potential decay rates of the positive plate as a function of sterilization time. Higher essentially irreversible open circuit potential of the sterilized positive plate as a function of time appears to be associated with changes in the oxygen over voltage characteristics. This phenomenon needs further studies. Gas chromatographic determinations of cell gases have shown that higher pressures in certain sterilized cells were due to oxygen. This suggests lower charge acceptance and/or lower rates of O_2-recombination. Some capacity lowering observed in certain experimental cells during characterization cycling has been caused by insufficient charge adjust resulting in negative limited cells under 100% d.o.d. Optimum charge adjust is being determined.

The 4AH factorial cells after sterilization have completed 207 deep cycles while 18 plate cells have completed 150 deep cycles with stable performance. These cells will be further characterized under various conditions of interest to J.P.L.

II. Battery Engineering:
The development of crimp polymeric (KEL-C) seal for heat-sterilizable and impact resistant Ni-Cd space cells was continued. The cause of leakage after sterilization has been identified as due to the flow of the polymer during heat-sterilization. Pre-treatment

of KEL-C does not eliminate this problem. Several design modifications have been evolved to eliminate the problem and the modified seals are under test. Hermeticity prior to heat-sterilization is excellent. A parallel effort using polypropylene in place of KEL-C is also underway as back up.

Cell design, pre-sterilization characterization and post-sterilization performance data (AH capacity, cell voltage at 50% d.o.d., end of charge voltage and pressure) for 25AH, prismatic and cylindrical cells, for up to 100 post-sterilization cycles are given. Except for slightly higher end of charge voltage no change in performance characteristics has been observed due to sterilization for up to 100 deep discharge cycles. Characterization of 20 prismatic cells (25AH) is underway. The long range testing program for 25AH cells to meet JPL mission requirements have been described.

III. Impact Testing of Cells and Components:
The high impact test facility has been extensively used to study existing Ni-Cd cells subject to shock environment.

The mechanical properties of the sintered positive and negative plates, the prime structural elements of the cell, have been determined. Material behavior under tension and compression loading has been established. Also, static and dynamic rates of loading have been used to better understand the transfer into impact loading response. The effects of electrolyte saturation and heat-sterilization on the mechanical properties of dry electrodes have been determined.

Present work includes the measurements of the static and dynamic bearing strength of the plates under controlled degrees of lateral restraint. Development of an experimental technique suitable to

measure general displacement as a function of time during impulsive loading is also underway.

1.0 Introduction

This is the eighth quarterly report on the heat-sterilizable, as well as heat-sterilizable and impact resistant Ni-Cd battery research and development under Jet Propulsion Laboratory Contract No. 951972 Modification No. 6. The program is sponsored under NASA Contract NAS-7-100, Task Order No. RD-26. The object of this contract is to perform research development and engineering work leading to the design, development, engineering, manufacture and testing of hermetically sealed, rechargeable Nickel-Cadmium cells capable of heat-sterilization as well as heat-sterilization and impact landing for space missions.

Since the last quarterly report, several modifications have been made in the technical portion of the work statement. The several tasks under the modified work statement may be grouped under the following three broad headings:

1. Electrochemistry of heat sterilizable cells. This will include basic research and development work on the positive and negative plates and separator as well as design, assembly and testing of complete cells leading to batteries capable of satisfactory operation after undergoing heat-sterilization.

2. Battery Engineering: This will include full size cell design development, optimization, production and testing of heat-sterilizable as well as heat-sterilizable and impact resistant cells. Initially two designs (a) cylindrical and (b) rectangular (prismatic) of 25 AH nominal capacity will be developed and evaluated. Hermetic seal design, assembly and testing to withstand the heat-sterilization as well as impact testing will be part of the bat-

tery engineering program.

3. Impact Testing of Cells and Components: Both static and dynamic testing of seals, cases, plates, and complete cells will be performed up to approximately 4000g in order to develop cells capable of hard impact landing missions.

The work performed during the eighth quarter is reported in above three separate sections.

I. HEAT STERILIZATION:

A. Prismatic, 4AH, 17 Plate, Factorial Cells:

During this quarter, these cells have satisfactorily completed 207 deep discharge (to 1.0 volt cut-off), post-sterilization cycles. Typical data for cycle numbers 166, 187 and 207 are given in Table I. Of the original 16 cells, seven cells containing Pellon polypropylene separator 14019 failed during post-sterilization cycling. The mode of failure in all cases was mechanical weakening of the separator (due to probable breakdown during heat-sterilization of the latex binder used in the manufacture of 14019 separator) and cadmium migration during post-sterilization cycling into the larger voids left in the separator. This resulted in electrical shorting of the cells and the cell failure. From the results of initial screening and this factorial experiment, it appears that of all the separator materials tested to date, the Pellon polypropylene type FT1140 appears most suitable for heat-sterilizable Ni-Cd cells. A critical parameter for sealed cells is the amount of pore fill. From the preliminary screening and pressure data on sealed cells which included 60, 70, 80 and 90% of pore fill (% of "free volume" filled with KOH), 70 and 80% were selected for the factorial experiment. The data of Table I-1 clearly show that 80% pore fill gives higher AH capacity on discharge and lower cell resistance. However, the effect of pore fill on the end of charge voltage appears to be negligible. These data do not show any significant difference between 30% and 34% KOH concentrations with 80% pore fill which has a major effect on capacity and cell resistance. The effect of KOH concentration on the performance of heat-sterilizable cells will have to be determined more accurately with additional cells. It will be noted that the end of charge voltage remains higher than for unsterilized cells. The cycling of these factorial cells will continue to 400 cycles at 100% d.o.d. or until failure, which ever occurs first.

TABLE I - 1

Ni-Cd Rectangular Cells, Factorial Design Experiment, 17 Plate

ELECTROCHEMICAL PERFORMANCE DATA

FOR FACTOR DESCRIPTION AND LEVELS SEE TABLE BELOW

Cell No.	Factors				Cycle No.	Charge Data						Discharge Data; 1.0V Cut Off				
	A	B	C	D		Amp.	Hrs.	AH Input	ECV Volts	ECP PSIA	ECR mΩ	Amp	AH Output	EDP PSIA	EDR mΩ	Eff. %
17	1	0	0	1	166	.400	17	6.8	1.458	---	18.06	2.0	3.118	----	42.36	62.9
19	1	0	0	1	166	.400	17	6.8	1.443	---	18.48	2.0	3.134	----	35.12	63.2
21	1	0	1	1	166	.400	17	6.8	1.464	---	11.21	2.0	3.634	----	12.43	73.3
23	1	0	1	1	166	.400	17	6.8	1.478	---	11.91	2.0	4.252	----	12.39	85.7
25	1	1	0	1	166	.400	17	6.8	1.470	---	15.35	2.0	3.266	----	52.30	65.8
27	1	1	0	1	166											
29	1	1	1	1	166	.400	17	6.8	1.470	---	10.37	2.0	4.000	----	12.24	80.6
31	1	1	1	1	166	.400	17	6.8	1.456	---	15.72	2.0	4.318	----	22.13	87.1

A: Separator Type
(0) = 14019
(1) = FT2140

B: KOH Conc.
(0) = 30 w/o
(1) = 34 w/o

C: % Pore Fill
(0) = 70%
(1) = 80%

D: Sterilization
(0) = Unsterilized
(1) = Sterilized

TABLE I-1 (cont'd)

Ni-Cd Rectangular Cells, Factorial Design Experiment 17 Plate

ELECTROCHEMICAL PERFORMANCE DATA

FOR FACTOR DESCRIPTION AND LEVELS SEE TABLE BELOW

Cell No.	Factors				Cycle No.	Charge Data						Discharge Data; 1.0V Cut Off				
	A	B	C	D		Amp.	Hrs.	AH Input	ECV Volts	ECP PSIA	ECR mΩ	Amp	AH Output	EDP PSIA	EDR mΩ	Eff. %
17	1	0	0	1	187	.400	17.0	6.8	1.473	--	17.33	2.0	3.184	--	34.09	64.2
19	1	0	0	1	187	.400	17.0	6.8	1.462	--	19.55	2.0	3.352	--	29.41	67.6
21	1	0	1	1	187	.400	17.0	6.8	1.467	--	11.09	2.0	3.834	--	10.59	77.3
23	1	0	1	1	187	.400	17.0	6.8	1.514	--	13.86	2.0	4.400	--	13.08	88.7
25	1	1	0	1	187	.400	17.0	6.8	1.471	--	15.01	2.0	3.234	--	40.87	65.2
27	1	1	0	1	187											
29	1	1	1	1	187	.400	17.0	6.8	1.448	--	10.45	2.0	4.166	--	10.34	84.0
31	1	1	1	1	187	.400	17.0	6.8	1.466	--	13.56	2.0	4.500	--	15.35	90.7

A: Separator Type
(0) = 14019
(1) = FT2140

B: KOH Conc.
(0) = 30 w/o
(1) = 34 w/o

C: % Pore Fill
(0) = 70%
(1) = 80%

D: Sterilization
(0) Unsterilized
(1) Sterilized

TABLE I-1

Ni-Cd Rectangular Cells, Factorial Design Experiment 17 Plate

ELECTROCHEMICAL PERFORMANCE DATA

For FACTOR DESCRIPTION AND LEVELS SEE below

Cell No.	Factors				Cycle No.	Charge Data						Discharge Data; 1.0V Cut Off				
	A	B	C	D		Amp.	Hrs.	AH Input	ECV Volts	ECP PSIA	ECR mΩ	Amp	AH Output	EDP PSIA	EDR mΩ	Eff. %
17	1	0	0	1	207	400	17	6.8	1.471	---	19.28	2.0	2.984	-----	39.76	60.2
19	1	0	0	1	207	400	17	6.8	1.460	---	22.62	2.0	3.200	-----	37.65	64.5
21	1	0	1	1	207	400	17	6.8	1.471	---	11.88	2.0	3.718	-----	11.78	75.0
23	1	0	1	1	207	400	17	6.8	1.536	---	16.93	2.0	3.734	-----	23.56	75.3
25	1	0	0	1	207	400	17	6.8	1.476	---	16.67	2.0	3.000	-----	46.69	60.5
27	1	0	0	1	207	400	17	6.8	1							
29	1	0	1	1	207	400	17	6.8	1.474	---	11.04	2.0	4.166	-----	11.90	84.0
31	1	0	1	1	207	400	17	6.8	1.470	---	14.04	2.0	4.418	-----	17.64	89.1

A: Separator Type
(0) = $14_{0}19$
(1) = FT2140

B: KOH Conc.
(0) = 30 w/o
(1) = 34 w/o

C: % Pore Fill
(0) = 70%
(1) = 80%

D: Sterilization
(0) = Unsterilized
(1) = Sterilized

B. Prismatic, 4AH, 18 Plate Cells:

It will be recalled that these cells were made to study the effect of cell-core compression on reproducibility of the cells. These cells have higher compression than the 17 plate cells. Also these cells have one more negative plate and therefore slightly greater negative to positive ratio. These cells have now undergone 150 deep discharge cycles after sterilization. Data from cycles in Table I-2 show that these cells continue to deliver high uniform capacity. Typically (cycle #100), 80% $\pm$ 3.2% of the positive formation capacity. Cycling will continue for 400 cycles or until failure, which ever occurs first.

C. Effect of RAI Treated Separator on Cell Performance:

This is the continuation of the work on RAI treated FT2140 separator that was reported in the last quarterly progress report. Specifically, it was important to see if this pretreatment improves post-sterilization cell performance.

Table I-3 lists the data from pre-sterilization cycles #12, #16, #20, #24 and #29 for the RAI treated and control cells. The higher ECP in the RAI cell remains higher than in the control cell. (124.7 p.s.i.a. versus 67.7 p.s.i.a. for the 29th cycle.) All cells have approached 80% utilization of the positive formation capacity. ECV as well as resistance values are similar.

After 29 pre-sterilization cycles, these cells were heat-sterilized at 135^{o}C for 64 hours. Post-sterilization characterization routine was identical to pre-sterilization characterization routine. During the sterilization, the RAI-#1 cell developed high resistance ($\sim$40mΩ) and did not undergo cycling. Therefore, only RAI #2 cell together with the two control cells were cycled. Pressure on RAI #2 and one of the control cells was monitored. Typical post-sterilization cycle data, up to 65 cycles, are given in Table I-4. These post-sterilization cycle data support the conclusion reached during the last quarter that no permanent improvement results from RAI

TABLE I - 2

Ni-Cd 18 Plate FT2140 Separator 30% KOH 80% Pore Fill

C.R. = C/12.5 C.L. = 137% D.R. = C/2.5 n = 4

POST STERILIZATION CYCLE DATA

Cycle #	ECV Volts Ave.	S	OCV Volts Ave.	S	ECR mΩ Ave.	S	EDR mΩ Ave.	S	Cap. (AH) Ave.	S	Effcy (%) Ave.	S
91	1.520	.003	1.423	.002	15.53	7.01	14.17	3.34	4.204	.152	84.8	3.1
95	1.469	.004	1.401	.002	15.99	8.54	16.34	7.50	4.046	.106	81.6	2.1
100	1.471	.006	1.396	.003	11.73	1.13	13.57	2.48	3.984	.143	80.3	2.9
105	1.458	.003	1.387	.004	11.43	.96	15.59	3.61	4.013	.159	80.9	3.2
110	1.453	.010	1.384	.009	12.08	1.23	15.05	3.24	3.967	.234	80.0	4.7
111	1.500	.007	1.434	.007	12.29	1.51	14.72	3.01	3.875	.250	78.1	5.0
115	1.486	.007	1.412	.003	11.34	1.04	13.66	3.11	4.025	.236	81.2	4.8
120	1.445	.016	1.375	.010	12.49	1.64	14.20	4.15	3.926	.380	79.2	7.7
125	1.487	.011	1.418	.005	13.62	3.92	16.53	6.02	4.042	.236	81.5	4.8
130	1.460	.011	1.389	.012	13.46	3.54	14.62	3.91	3.842	.413	77.5	8.3
131	1.455	.017	1.394	.016	12.42	2.34	14.62	5.20	3.737	.529	75.4	10.7
135	1.464	.007	1.399	.008			15.68	5.65	4.009	.355	80.8	7.2
140	1.462	.006	1.398	.009	13.67	2.86	16.45	6.49	3.992	.334	80.5	6.7
145	1.467	.006	1.384	.011	13.76	3.14	18.83	7.87	3.979	.293	80.2	5.9
150	1.469	.008	1.417	.007	15.28	4.34	19.40	8.39	4.184	.158	84.4	3.2

TABLE I - 3

EFFECT OF RAI TREATED SEPARATOR

PRE STERILIZATION

Ni-Cd 18 Plate FT2140 Separator 30% KOH 80% Pore Fill

C.R. = c/12.5 C.L. = 137% D.R. = c/2.5

Separator Type	Cell #	Cycle #	ECV Volts	ECR m Ω	EDR m Ω	ECP psia	EDP psia	ECC AH	Effcy. %
RAI	1	12	1.433	10.72	11.14	114.7	14.7	3.652	73.6
RAI	2	12	1.435	10.40	10.77			3.934	79.3
Control	1	12	1.432	9.94	12.41	82.7	14.7	3.634	73.3
Control	2	12	1.436	10.28	11.69			3.887	78.3
RAI	1	16	1.455	12.22	12.55	134.7	42.7	3.852	77.7
RAI	2	16	1.454	11.43	11.78			3.984	80.3
Control	1	16	1.461	13.71	15.02	42.7	14.7	4.166	84.0
Control	2	16	1.454	12.90	13.00			4.034	81.3
RAI	1	20	1.437	11.41	15.00	118.7	44.7	3.566	71.9
RAI	2	20	1.433	10.67	14.11			3.800	76.6
Control	1	20	1.441	12.34	19.03	54.7	44.7	4.000	80.6
Control	2	20	1.441	12.00	15.42			4.000	80.6
RAI	1	24	1.429	12.26	13.66	118.7	52.7	3.584	72.3
RAI	2	24	1.430	11.31	12.69			3.934	79.3
Control	1	24	1.435	12.77	19.44	52.7	44.7	3.934	79.3
Control	2	24	1.431	12.49	14.23			4.052	81.7
RAI	1	29	1.451	11.78	13.14	124.7	67.7	3.918	79.0
RAI	2	29	1.441	10.89	12.10			4.016	81.0
Control	1	29	1.449	12.55	18.01	48.7	14.7	4.084	83.7
Control	2	29	1.447	11.95	13.30			4.152	81.5

TABLE I - 4

EFFECT OF RAI TREATED SEPARATOR

POST STERILIZATION

Ni-Cd 18 Plate FT2140 Sep. 30% KOH 80% Pore Fill

C.R. = C/12.5 C.L. = 137% D.R. = C/2.5

Separator Type	Cell #	Cycle #	ECV Volts	ECR m Ω	EDR m Ω	ECP psia	EDP psia	ECC AH	Effcy. %
RAI	2	1	1.496	11.65	11.14	--	--	3.434	69.2
Control	1	1	1.503	15.45	19.94	54.7	--	3.084	62.2
Control	2	1	1.499	16.18	15.22	--	--	3.152	63.5
RAI	2	3	1.477	11.12	11.19	54.7	14.7	3.200	64.5
Control	1	3	1.473	13.04	15.46	104.7	18.7	2.700	54.4
Control	2	3	1.515	16.66	17.26	--	--	2.852	57.5
RAI	2	7	1.465	9.44	11.90	94.7	14.7	2.984	60.2
Control	1	7	1.471	10.52	16.69	104.7	25.7	2.566	51.7
Control	2	7	1.479	15.38	19.53	--	--	3.100	62.5
RAI	2	15	1.471	10.79	11.38	81.7	14.7	3.352	67.6
Control	1	15	1.475	11.69	16.96	97.7	24.7	2.852	57.5
Control	2	15	1.492	16.70	20.52	--	--	3.666	73.9
RAI	2	25	1.464	--	10.65	73.7	14.7	3.518	70.9
Control	1	25	1.460	--	19.20	75.7	19.7	2.934	59.2
Control	2	25	1.459	--	18.37	--	--	3.518	70.9
RAI	2	35	1.469	11.58	12.34	68.7	14.7	3.634	73.3
Control	1	35	1.463	12.03	23.38	67.7	21.7	3.000	60.5
Control	2	35	1.465	24.94	31.09	--	--	3.584	72.3
RAI	2	45	1.468	11.62	12.26	62.7	14.7	3.684	74.3
Control	1	45	1.459	12.31	24.86	58.7	18.7	3.084	62.2
Control	2	45	1.463	24.46	42.02	--	--	3.652	73.6
RAI	2	55	1.471	12.04	11.36	59.7	14.7	3.752	75.6
Control	1	55	1.457	12.63	22.66	56.7	18.7	3.118	62.9
Control	2	55	1.467	31.06	32.59	--	--	3.684	74.3

eatment of FT2140. No further work is, therefore, planned th this RAI treated separator as indicated in the last report.

D. Single Electrode Potential Studies in the Cell Environment: the last quarterly report, the development and design of a /HgO reference electrode for study of the individual electrode larizations in cell environment was described. This reference electrode was modified during this quarter as shown in Fig. I-A. The gas passage is now by way of a slot cut into the threads enabling us to go back to the original thread size. By off-setting the reservoir the gas passage may now continue up through the body of the electrode close to its axis. These improvements should enable us to make simultaneous pressure and reference voltage measurements on existing cells while reducing the problems of leakage and breakage. This reference electrode design has been successfully used to study the individual electrode behavior in "sealed cell" environments.

E. End of Charge and Open Circuit Stand Voltage:
Experiments were continued with 6 of the 8 cells (two had shorted see 7th quarterly report) which had been sterilized for 0, 1, 2, 4, 8, 16, 32 and 64 hours. The self-discharge rate expressed as a function of open circuit cell voltage vs. stand time following a c/12.5, 137% charge was determined for these cells. Data is plotted in Figure I-B. There does not appear to be any correlation between sterilization time and cell voltage level or rate of descent during open circuit stand following charge. The only comment to be made is that the one unsterilized cell has an open circuit voltage considerably lower than any of the sterilized cells.

End of charge voltage data using a reference electrode had indicated that excess voltage rise near the end of charge for sterilized cells can be attributed to the behavior of the positive electrode. To supplement this data, a study of end of charge,

FIGURE 1 - A

An Hg/HgO Reference Electrode Design for "Sealed Cell" Studies

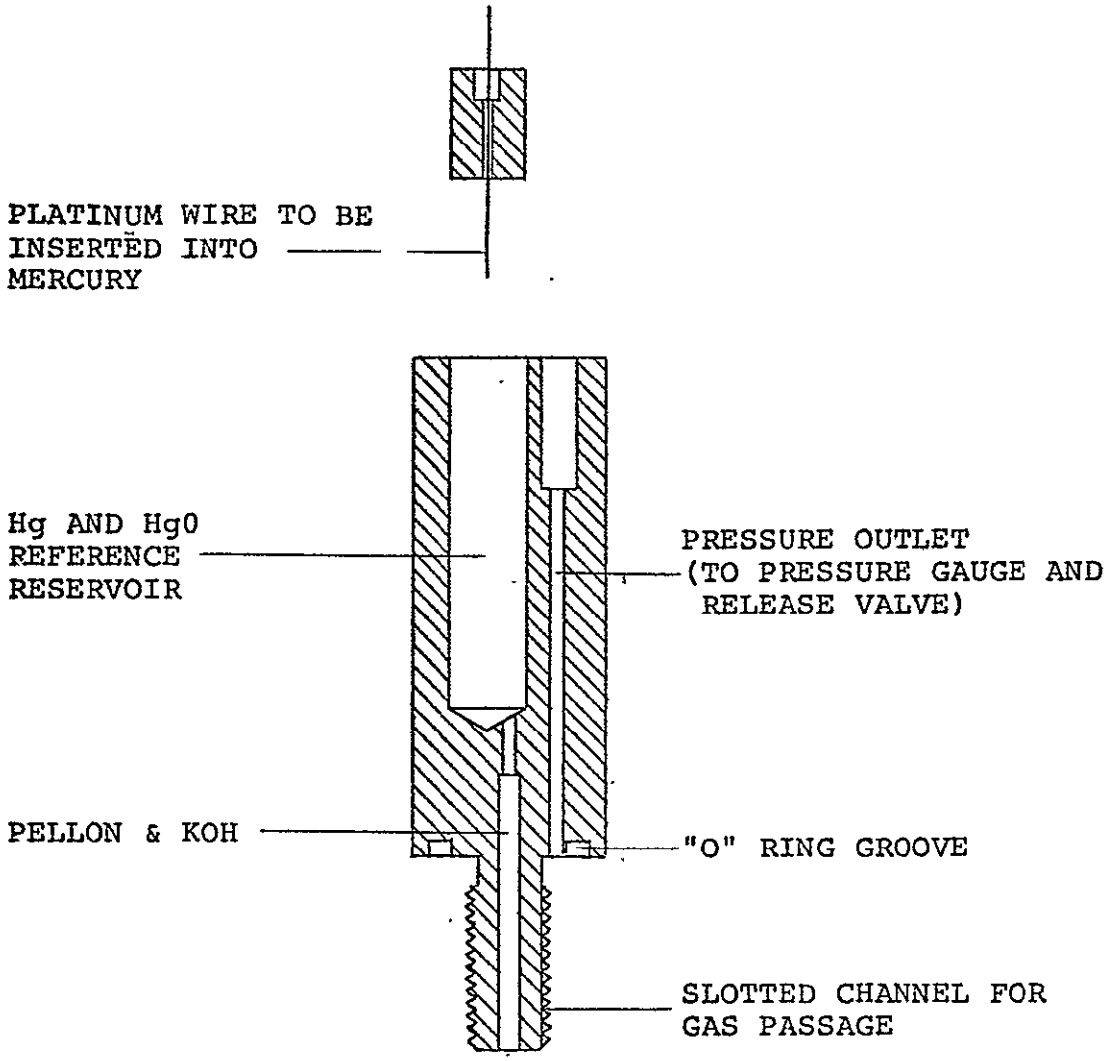

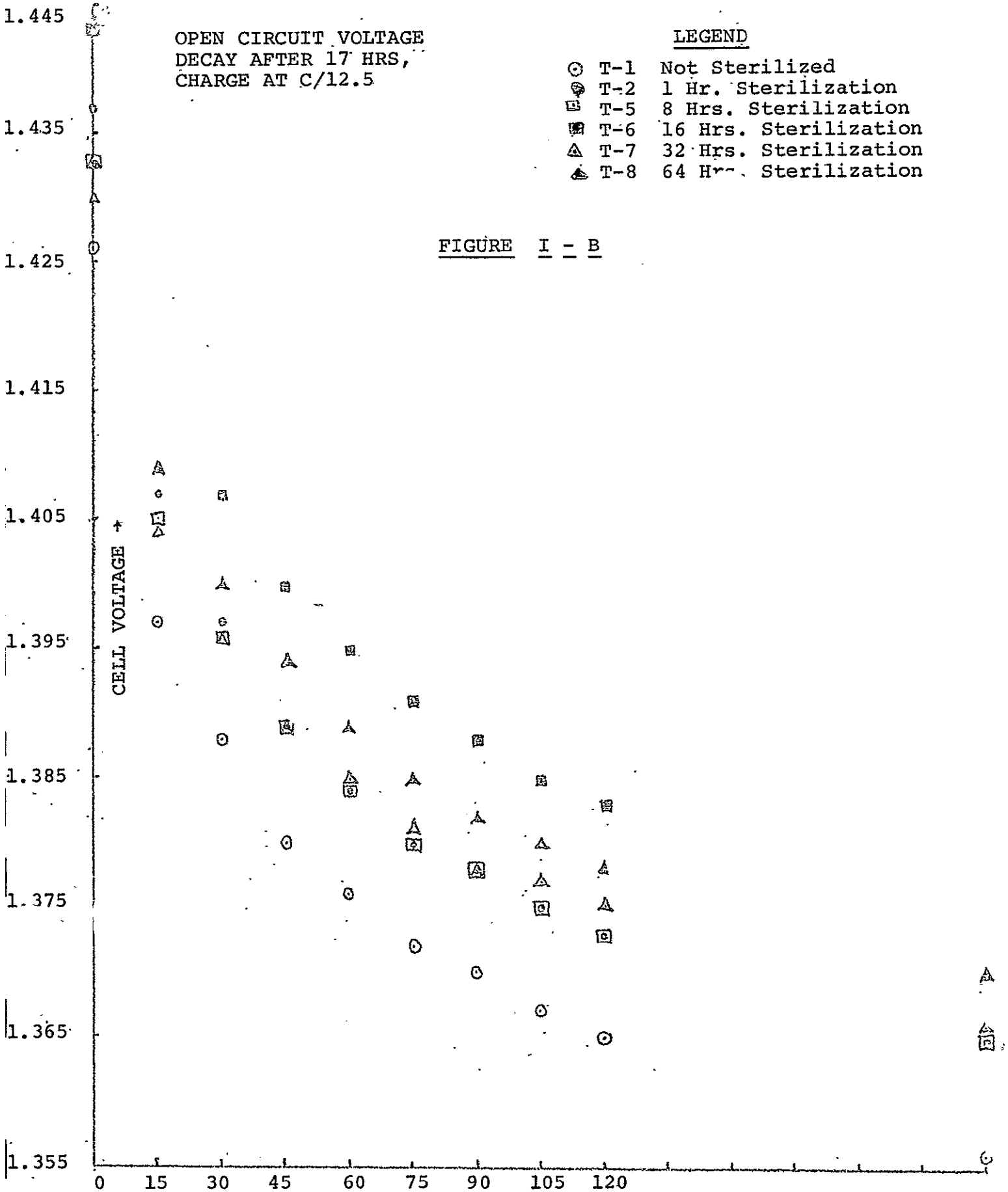
OPEN CIRCUIT VOLTAGE
DECAY AFTER 17 HRS,
CHARGE AT C/12.5
LEGEND
T-1 Not Sterilized
T-2 1 Hr. Sterilization
T-5 8 Hrs. Sterilization
T-6 16 Hrs. Sterilization
T-7 32 Hrs. Sterilization
T-8 64 Hrs. Sterilization
CELL VOLTAGE
1.445
1.435
1.425
1.415
1.405
1.395
1.385
1.375
1.365
1.355
0
15
30
45
60
75
90
105
120
TIME (MIN.)

FIGURE I - B

OCV and OCV decay was made. A mercury-mercuric oxide reference electrode previously described which would allow for cells to maintain sealed condition was inserted into the cells which were then brought to the standard fully charged condition (137%, c/12.5). Table I-5 lists the end of charge voltages for full cell and positive to reference as measured (negative to reference was calculated).

TABLE I - 5
End of Charge Voltages

Cell	Sterilization Time	Cell	Positive to Reference	Negative to Reference
T-1	0 hrs.	1.428 v.	.520 v.	-.908 v.
T-2	1 hr.	1.429 v.	.568 v.	-.861 v.
T-5	8 hrs.	1.469 v.	.568 v.	-.901 v.
T-6	16 hrs.	1.448 v.	.546 v.	-.902 v.
T-7	32 hrs.	1.452 v.	.565 v.	-.887 v.
T-8	64 hrs.	1.466 v.	.592 v.	-.874 v.

It can be seen that a marked difference exists between the end of charge, positive to reference voltage for all sterilized cells and the one unsterilized cell. (In future studies reference data will be obtained for a group of sterilized and unsterilized cells). The data in Table I-6 show that differences exist between sterilized and unsterilized positive with respect to open circuit voltage as well as end of charge voltages. Although oxygen potential decay on open circuit does contribute to observed OCV, it appears that differences exist between the sterilized and non-

sterilized positives which go beyond that of mere oxygen over-voltage phenomenon.

TABLE I - 6

Open Circuit Stand Voltages vs. Time

Cell	Cell Voltage 6 min.	Cell Voltage 4½ hr.	Positive to Ref. 6 min.	Positive to Ref. 4½ hr.	Negative to Ref. 6 min.	Negative to Ref. 4½ hr.
T-1 (0)*	1.392v.	1.344v.	.500v.	.459v.	-.892v.	-.885v.
T-5 (8)	1.433v.	1.365v.	.540v.	.472v.	-.893v.	-.893v.
T-7 (32)	1.420v.	1.344v.	.548v.	.484v.	-.872v.	-.860v.
T-8 (64)	1.406v.	1.344v.	.568v.	.508v.	-.838v.	-.834v.

* Sterilization time in hours.

The data also indicate the stability of the negative electrode during stand and the greater instability of sterilized positive as compared to the unsterilized positive. The unsterilized positive drops 41 mv during this stand (between 6 min. and 4½ hrs.) while the three other cells drop between 68 and 60 mv during that same stand time. The greatest drop in the negative was 12 mv. Open circuit decay data for the positive electrode was obtained for all six cells following the standard charge and plotted as voltage vs. log time. These plots appear in Figures I-C and I-D. Two separate decays were run for cell T-1. The slopes of the E vs. log T plots are reasonably alike for all sterilized cells. The one unsterilized cell indicated a difference in the second slope b^1. The values of the slopes are given in the table I-7.

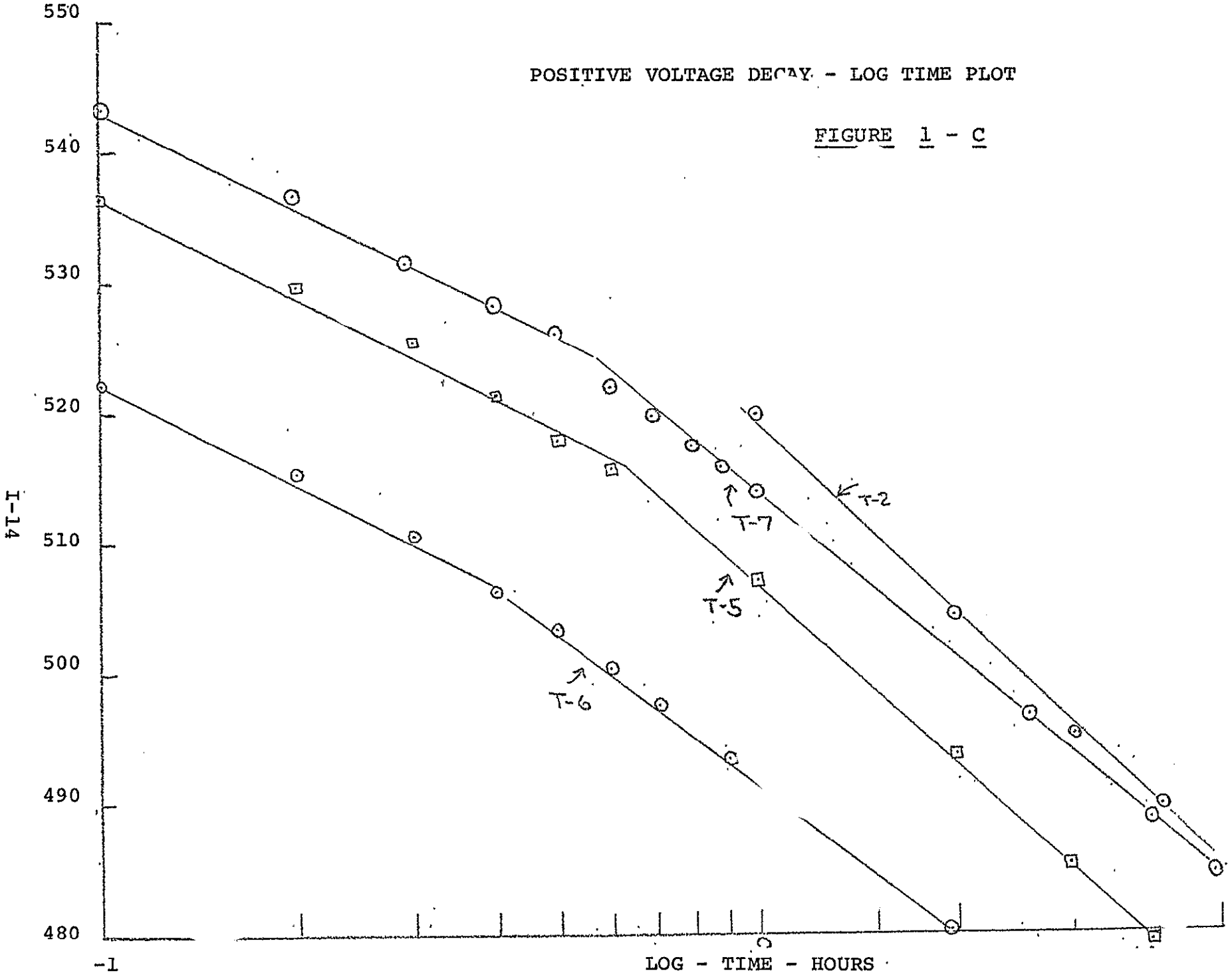
POSITIVE VOLTAGE DECAY - LOG TIME PLOT
FIGURE 1 - C
550
540
530
520
510
500
490
480
T-7
T-2
T-5
T-6
-1
0
LOG - TIME - HOURS

POSITIVE VOLTAGE DECAY - LOG TIME PLOT

FIGURE 1 - D

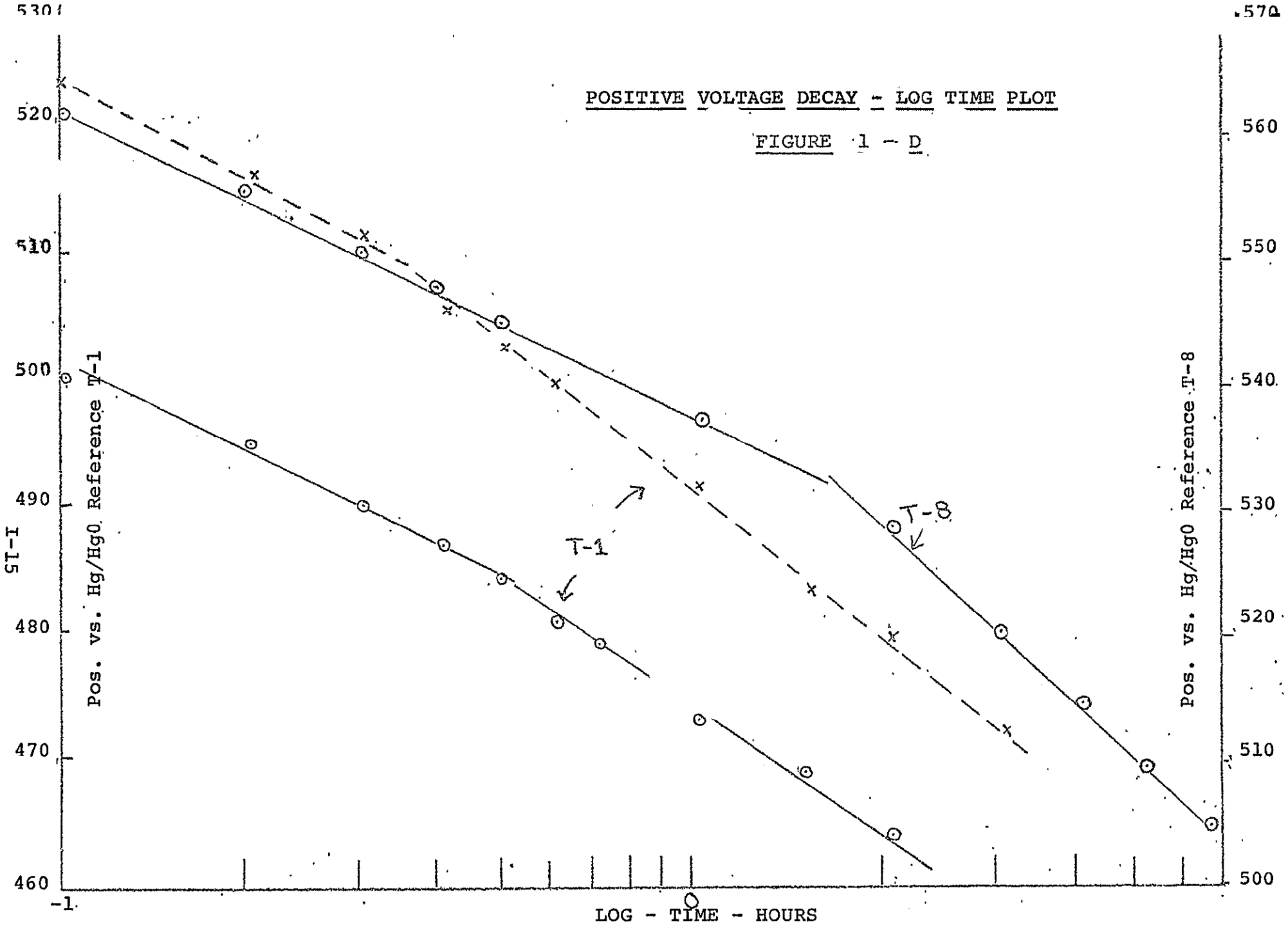

TABLE I - 7

Cell No.	b	b^1
T-1	Run 1: 26	35
	Run 2: 23	30
T-2	Not Recorded	42
T-5	25	39
T-6	26	39
T-7	25	40
T-8	25	47

$b = \frac{mv}{\text{Time decade}}$

The initial slope represents the first hour of open circuit time, the second slopecorresponds to decay beyond 1 hour.

A further discussion or theoretical interpretation must wait until more data is available on this phase of the work.

F. Cell - Discharge - Positive/Negative - Capacity Ratio: All 6 cells mentioned above were discharged to reversal, following a standard charge, at the C/12.5 rate. This data was obtained for the first two cycles following those cycles described in the preceding Quarterly Report and corresponds to the second and third discharge after charge adjust had been made. Capacity data and each electrode potential appear in Table I-8.

Table I - 8

Cell #	Ster. Time	Negative	Positive	Stand
T-1	0 hrs.	3.53 AH	4.07 AH	64 hrs.
T-2	1 hr.	3.63 AH	4.20 AH	64 hrs.
T-5	8 hrs.	4.07 AH	4.40 AH	5.25 hrs.

TABLE I - 8 (con't.

Cell #	Ster. Time	Negative	Positive	Stand
*T-6	16 hrs.	4.00 AH	4.40 AH	4.5 hrs.
*T-7	32 hrs.	4.00 AH	4.33 AH	4.5 hrs.
T-8	64 hrs.	3.70 AH	4.65 AH	5.25 hrs.

*T-6 and T-7 = third cycle after charge adjust by vented cycle.
All the rest - 2nd cycle after charge adjust.

In all cases the cells are negative limiting but had been positive limiting on previous discharges (see 7th quarterly report). This suggests a capacity change of the negative electrode during cycling. This may involve the separator system and/or electrolyte. This observed change in negative capacity will be investigated with freshly prepared cells with electrolyte starved and flooded, before and after sterilization.

G. Method for the Determination of Cell Gas Composition:
In support of investigations into the generation of hydrogen in sealed cells a gas chromatographic method has been developed which will enable us to determine the composition of 0_2, H_2, N_2 and Ar gas mixtures. The capabilities of the method are summarized in Table I-9.

TABLE I - 9

Gas	Analytical Range for 0.5 cc Sample at 1 atm. From V/0	To V/0	Relative Sensitivity H_2 = 1	Coefficient of Variation %	V/0
H_2	1.	80.	1	5.4	2.69
N_2	0.1	100.	41	1.8	94.60
0_2	0.1	100.	67	0.8	1.08
Ar	0.1	10.	69	.9	1.63

The analysis for 0_2, N_2 and Ar show excellent sensitivity and precision. The results for hydrogen, while not as good, should be adequate for this investigation.

The operating conditions are listed in Table I-10.

A column of Porapak Q in dry ice separates the components which are then detected by changes in thermal conductivity. The integrated response of the detector was found to be linear function of the number of moles 0_2, N_2 and Ar in the sample using the standards listed in Table I-11. The response to H_2, however, is non-linear and the sample size must be reduced for high hydrogen concentrations.

TABLE I - 10

Analysis of Battery Gases
by
GLC

EQUIPMENT: Instrument: Aerograph 1720-1 column switching valve, recorder with disc integrator.

Columns: "A" before column switching valve - 6' x 1/8" SS - Poropak N.

"B" after column swithcing valve outside oven - 17' x 1/8" SS - Poropak Q

"C" after column switching valve inside oven - 1' x 1/8" SS - Poropak N

Temperatures: Injector - ambient
Detector - 135°C
Columns - A and C ambient with temperature programming if analysis of other than fixed gases required - B - in dry ice (-78°C)

Detector: 150 milliamps

Gas: 30cc/min. - Helium

Syringes: Use only the 1.0 ml "Pressure-Lok" syringe made by Precision Sampling Co.

CALIBRATION: Calibration curves of integrator counts vs. moles of gas have been prepared for hydrogen, nitrogen, oxygen and argon.

TABLE I - 11

Calibration Standards for Analysis of Battery Gases

Cylinder	Vol. %					Wt. %			
#	N_2	O_2	H_2	Ar		N_2	O_2	H_2	Ar
1	93.46	2.12	1.10	3.32		92.82	2.40	0.08	4.70
2	88.45	8.80	-	2.75		86.36	9.81	-	3.83
3	82.30	15.3	-	2.40		79.75	16.93	-	3.32
4	94.60	1.08	2.69	1.63		96.19	1.25	0.20	2.36
5	91.07	-	7.85	1.08		97.74	-	0.61	1.65
6	79.49	-	18.7	1.81		95.29	-	1.61	3.09
7	51.71	-	47.0	1.29		90.83	-	5.94	3.23
8	68.43	-	31.1	0.47		95.92	-	3.14	0.94
9									

Standard #4 was run three times in two weeks to establish the precision and sensitivity data presented above. Figure I-E, a tracing of a typical chromatographic recorder chart, shows that complete separation of the components is made in 12 minutes. Total time for analysis including sampling and calculations is approximately 16 minutes.

Sampling of the cell gases is accomplished using a 0-1cc pressure-lok gas syringe (Precision Sampling Corp. #306001-A). The needle of the syringe is inserted through the cap and rubber septum of the fitting shown in Figure I-F. This device can be screwed into the vent hole of our experimental cells or into a "T", also shown in Figure 1-F, which in turn can be screwed into the cell. The "T" enables us to simultaneously measure pressure while sampling the gas. After introduction of the desired volume of gas into the syringe the valve on the syringe is closed and the needle withdrawn. Under these conditions, of sampling the number of moles of gas sample taken is a fixed fraction of the number of moles of the gas in the cell regardless of the cell pressure.

$$\text{fraction removed} = \frac{Vs}{Vs + Vc}$$

where Vs = volume in syringe - typically 0.50 cm^3

Vc = volume of cell - typically 23 cm^3

The sample is introduced into the gas chromatograph by reversing the above procedure i.e. insert needle through inlet septum of the chromatograph, open valve and inject.

G. Hydrogen Analysis in Cells with High ECP:

Using this technique, samples of gas from four cells have been analyzed on two different days. The results are shown in Table I-12. The two 25AH cells had developed high pressures at the end-of-charge, in excess of 200 p.s.i.a. The 4AH RAI cell had developed end-of-charge pressures of approximately 120 p.s.i.a. (see section I-C) while the 4AH control cell pressure was approximately 70 p.s.i.a.

FIGURE I - E

GC Curve

Std. #4

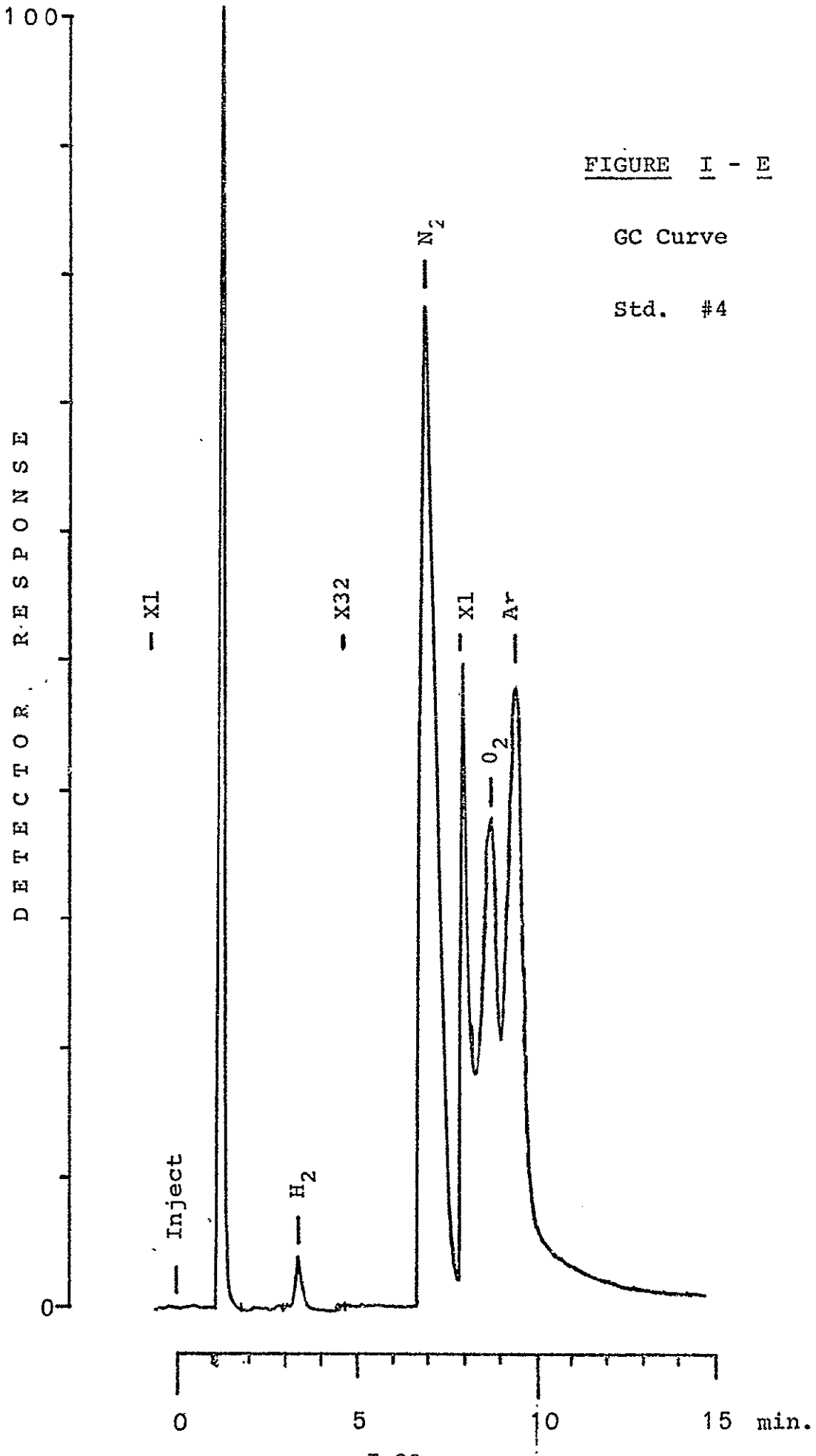

FIGURE 1 - F

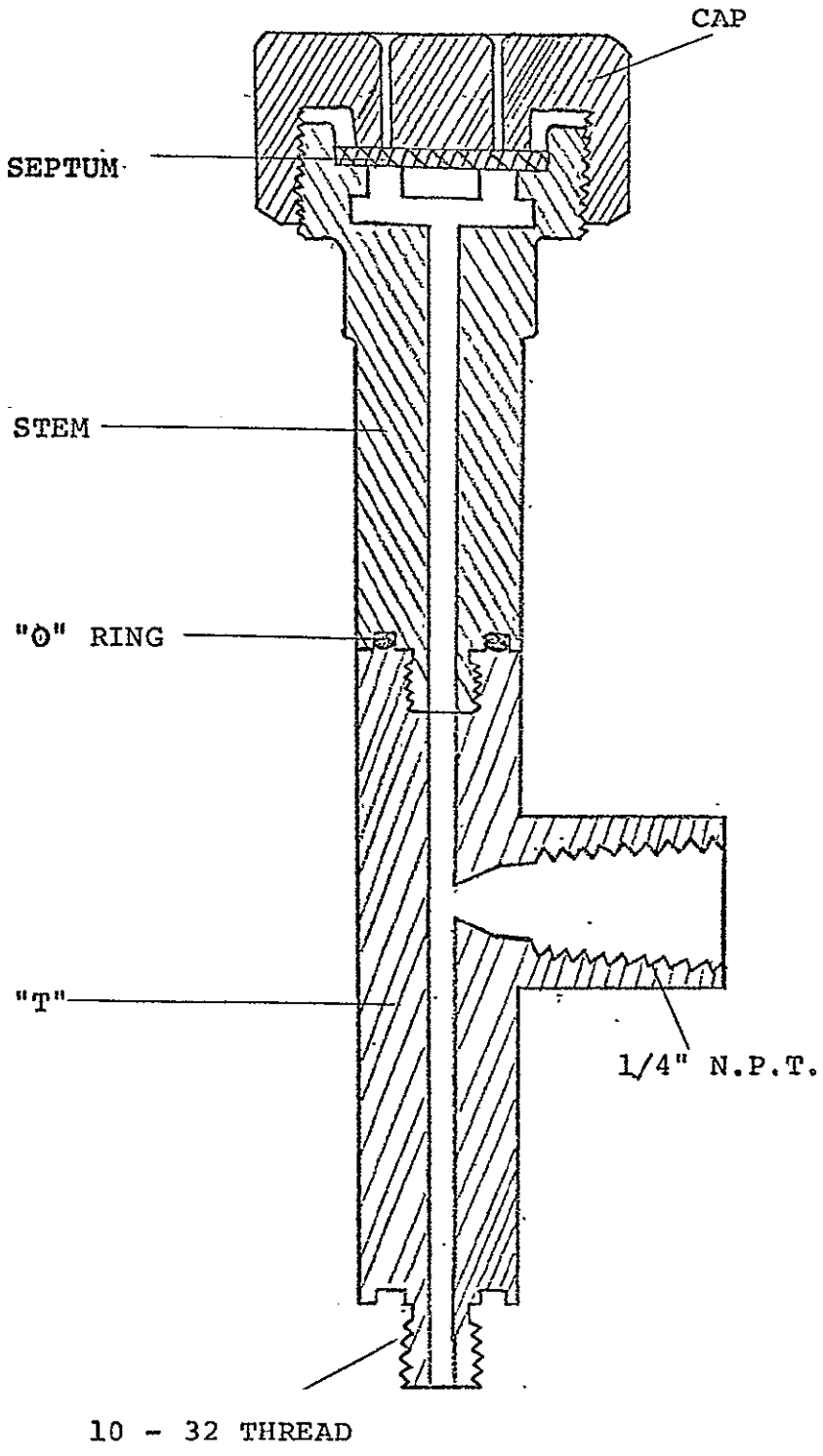

All cells contain hydrogen but in amounts equivalent to less than 0.5 p.s.i.a. The 25AH cells contain 4 to 5 times as much hydrogen as the 4AH cells, not greatly different from the ratio of the capacities. The presence of hydrogen in all cells shows that the method had adequate sensitivity and implies that presence of small amounts of hydrogen is to be expected in all cells.

The difference in nitrogen content in samples taken on the 17th of April compared to samples taken on the 15th reflects the fact that the cells were vented following introduction of air for determination of the cell volume after the first sample was taken. The wide variation in oxygen content reflects the differing extents of recombination which have occurred during charging and stand.

TABLE I - 12

ANALYSIS OF GASES IN CELLS WITH HIGH END OF CHARGE PRESSURE

Cell	Size Nom.	Vol. cm^3	Date	25°C Pressure Calcu'd psia	25°C Pressure Meas'd psia	10^{-5} Moles H_2	10^{-5} Moles N_2	10^{-5} Moles O_2	10^{-5} Moles Total	H_2 AH	O_2 AH	v/o H_2	v/o N_2	v/o O_2
P3	25 AH	57	4/15	11.1	<15	4.4	99.1	78.7	182.2	.0024	.084	2.4	55.0	42
P3	25 AH	57	4/17	12.2	<15	3.6	15.7	182.0	200.3	.0019	.195	1.8	7.8	90
P4	25 AH	57	4/15	12.2	<15	7.5	102.0	91.5	201.0	.0040	.098	3.7	51.0	46
P4	25 AH	57	4/17	28.8	30	4.9	171.0	294.0	469.9	.0026	.314	1.4	36.0	63
RAI-1	4 AH	23	4/15	17.5	17	1.7	19.1	92.2	113.0	.00092	.099	1.5	17.0	82
RAI-1	4 AH	23	4/17	30.7	36	1.6	37.7	155.0	194.3	.00086	.165	0.83	19.0	80
C-1	4 AH	23	4/15	12.3	19	1.05	41.8	36.5	79.4	.00056	.039	1.3	53.0	46
C-1	4 AH	23	4/17	3.6	4	0.78	15.6	6.7	23.1	.00042	.007	3.4	67.0	29

II Cell Design, Construction and Evaluation

A. Seal Development

Early in this reporting period several seals were assembled. The seal size and other pertinent data are shown in TABLE II-1

TABLE II-1

No	Seal Size	Crimp Press (PSI)	Final Dia (in.)	Pre Heat Sterilization Leak Rate (std cc/sec/atm)		Post Heat Sterilization Leak Rate (std cc He/sec/atm)
				air	He	
1	03	1300	.427	2.5×10^{-8}	1.4×10^{-7}	70μ
2	03	1300	.427	2.6×10^{-8}	9.6×10^{-7}	100μ
3	03	1300	.427	3.2×10^{-8}	3.2×10^{-8}	----
4	03	1000	.434	3.5×10^{-8}	3.5×10^{-8}	1×10^{-6}
5	03	1000	.434	3.9×10^{-8}	3.9×10^{-8}	90μ
6	03	1000	.434	4.3×10^{-8}	4.3×10^{-8}	----
7	04	1300	.503	2.9×10^{-8}	3.1×10^{-8}	90μ
8	04	1300	.503	4.2×10^{-8}	4.2×10^{-8}	80μ
9	04	1300	.503	5.0×10^{-8}	5.0×10^{-8}	----
10	04	1000	.509	4.4×10^{-8}	4.4×10^{-8}	70μ
11	04	1000	.509	4.6×10^{-8}	4.6×10^{-8}	70μ
12	04	1000	.509	5.2×10^{-8}	5.2×10^{-8}	----
A	04	1000	.509	----------	----------	∿10μ gross leak
B	04	1000	.509	----------	----------	∿ 8μ gross leak

Before heat sterilization the seals were generally leak tight as noted. After heat sterilization (135°C for 72 hours) all seals were gross leakers excepting seal number 4.

Examination of seals (including cross sectioning) reveals an axial extrusion of the KEL-F insulator leaving a leak path along the thread.

Four of these leakers were re-crimped on dies that were ground an additional .010" to allow additional reduction of the seal diameter and produce increased hydrostatic pressures

within the seal. One of these assemblies did reseal during this operation with a leak rate in the same order of magnitude (10^{-8} std cc He/sec/atm) as before. The three other assemblies did not reseal to the same degree, however their leak rate was reduced measurably. These tests indicate the thread form of the KEL-F is not destroyed during the heat sterilization process and loss of hermeticity is caused by flow of material out of the seal area. This flow decreases the pressures induced during the crimping process and failure results.

To determine if the extrusion of the KEL-F could be avoided by a heat treating process, these same assemblies were heat sterilized for a second time. As a result, the seals tested once again became gross leakers. It is therefore surmised that the flow of the KEL-F material is caused by the heating processes which soften the polymer and is aided by the forces generated within the seal during the crimping process. Therefore this material flow is considered a repetitive process which can not be eliminated by heat treating processes.

The next seal configuration incorporated a tapered top which was designed to restrict the movement of KEL-F out of the seal during the heat sterilization process. Also a thin flange with a weld projection was included which allowed for an easier and more reliable flange to cell cover joint.

Ten seal assemblies were made of this type in the 04 size category. The weld flange gave a hermetic joint in most cases but a thinner flange and a smaller diameter weld projection should further improve the design. A smaller diameter flange will be used for the prismatic cell top.

Prior to heat sterilization the seal had leak rate in the 10^{-8} range. Six of these seal assemblies that were crimped on the ends, as well as along the axis, were found to be gross leakers at ∿10μ vacuum after heat sterilization.

Visual examination of the assembly shows that this end crimp retention design was only partially effective.

A cross section of this seal revealed a small but full length leak path along the threads on both sides similar to previous observations.

Other design changes were then made. These included a reduction in the cross section of polymeric insulator, designed to reduce material flow, a rolled outer sleeve lip design to further restrict polymer flow out of the seal area and a blind thread at the bottom of the outer sleeve to restrict polymer flow in that direction. A schematic diagram of the seal is shown in Figure II-A. Also included in the new design was the use of polypropylene as an alternate material for use as a seal. Seals of this design are presently being fabricated and will be evaluated during the next reporting period.

B. Prismatic Cells

The testing of engineering development cells continued this quarter. The data produced by these cells (previously reported as cells P-1 through P-4 plus other cells fabricated since the last reporting period) was used to generate final design parameters. In this group are cells which are both heat sterilized and non heat sterilized and which contain nylon and polypropylene separators. The performance of these cells is described.

The polyamide separator containing cell performance data is shown in Figure II-B. The plate size and plate material are identical to those used in other cells containing polypropylene

Figure II-A
CRIMPED POLYMERIC SEAL

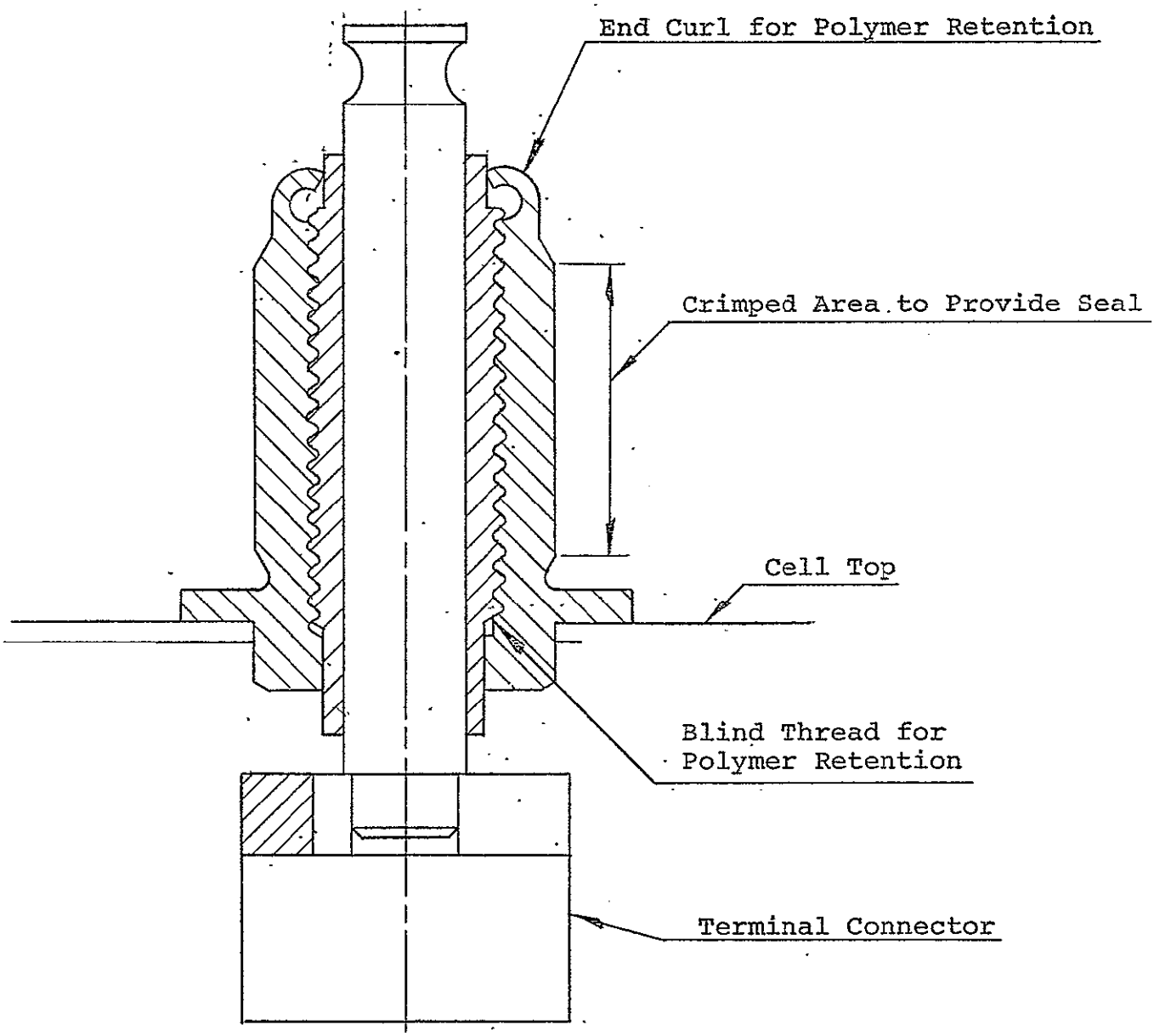

TEXAS INSTRUMENTS
INCORPORATED
ATTLEBORO, MASS., U.S.A

SCHEMATIC REPRESENTATION
HEAT STERILIZEABLE
CRIMPED POLYMERIC SEAL

Figure II-B

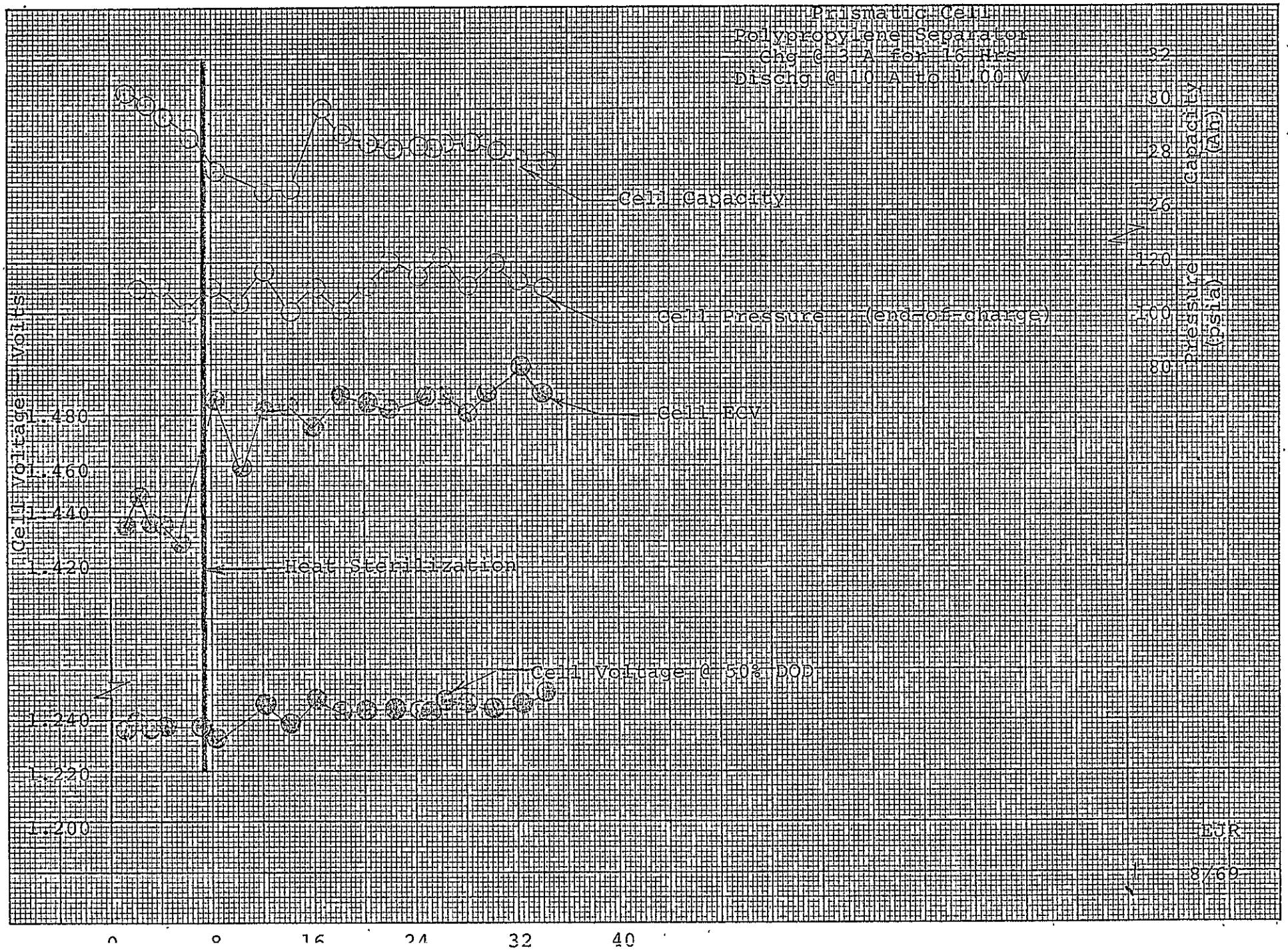
Prismatic Cell
Polypropylene Separator
Chg @ 3 A for 16 Hrs
Dischg @ 10 A to 1.00 V
Cell Capacity
Cell Pressure (end of charge)
Cell ECV
Heat Sterilization
Cell Voltage @ 50% DOD
Cell Voltage - Volts
1.480
1.460
1.440
1.420
1.240
1.220
1.200
32
30
28
26
120
100
80
Pressure (psia)
Capacity (Ah)
0
8
16
24
32
40
Cycle No.
EJR
8/69

separator. Thus performance characteristics are affected by the separator and some mechanical differences as explained in the previous quarterly report. The variations in cell capacity are a result of fluctuations in the test temperature and exceptions to the duty cycle described in the figure. At the 10 ampere discharge rate at 70°F the cell has a specific energy of 15.5 watt-hours per pound.

The polypropylene separator containing, non heat sterilized cell performance data is presented in Figure II-C. The delivered capacity is similar to that observed for the cell containing polyamide separator. The end-of-charge cell pressure is higher than cells with polyamide separator and reflects the smaller recombination rate constant observed for cells with polypropylene separators of this type. The slightly lower discharge voltage results in a lowered specific energy of 14.5 watt-hours per pound.

The heat sterilized polypropylene separator cell performance data is shown in Figure II-D. Pre heat sterilization data is comparable to that previously described with the exception of end-of-charge cell pressure. This effect is caused by a higher than designed electrolyte fill level. Post heat sterilization behavior is characterized by some loss in cell capacity. This is now believed caused by the cell becoming negative limited during discharge and is a result of the free cadmium metal being oxidized to cadmium hydroxide during heat sterilization. The effect of negative limitation, during discharge, is to reduce the cell capacity deliverable to 1.00 volts. As discussed in earlier reports the increase in end-of-charge cell voltage is associated with the positive electrode and is not an indicator of hydrogen evolution. This fact was verified by analyzing the cell atmosphere by gas chromatographic techniques.

Figure II-C

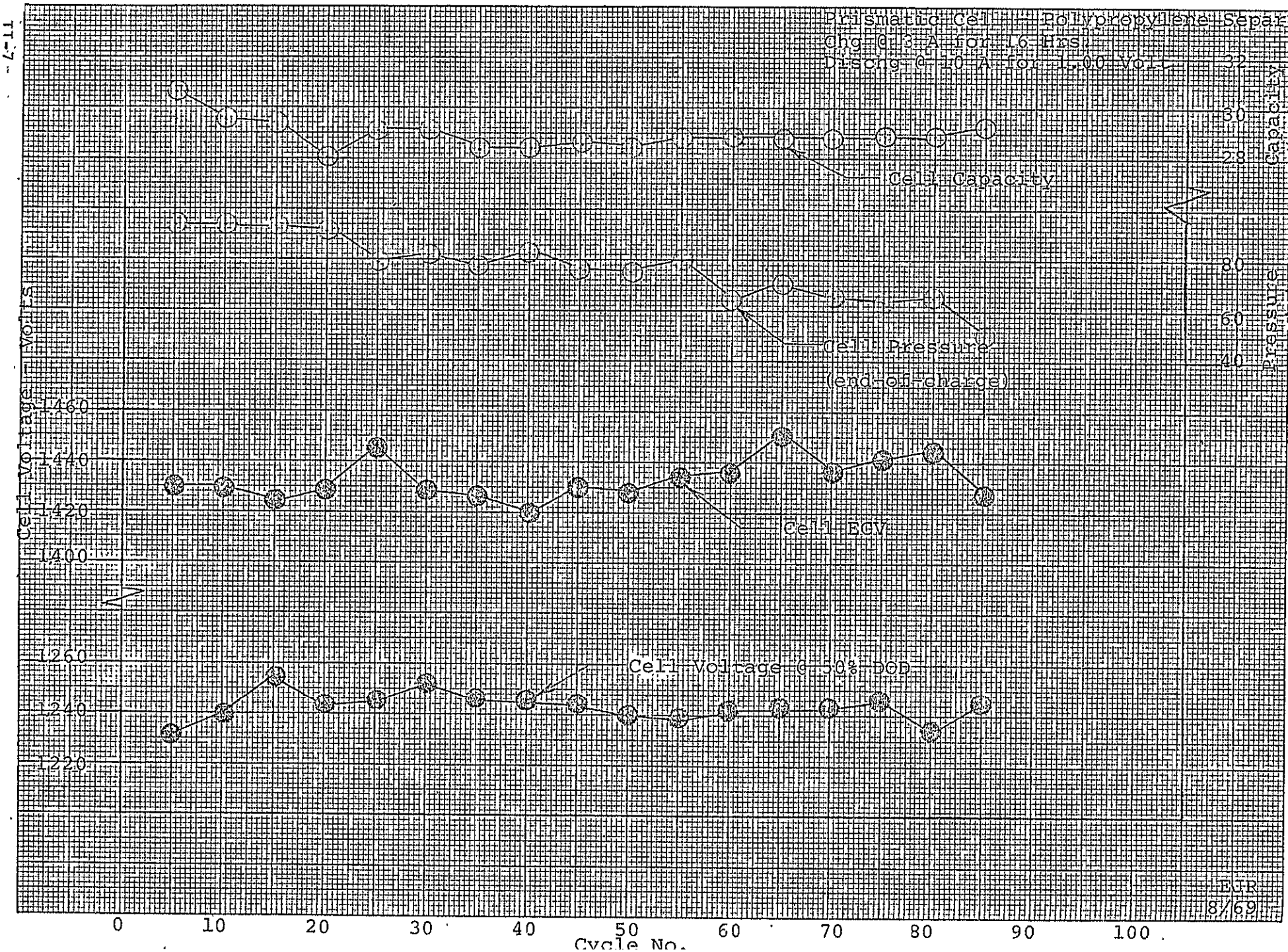

Figure II-D

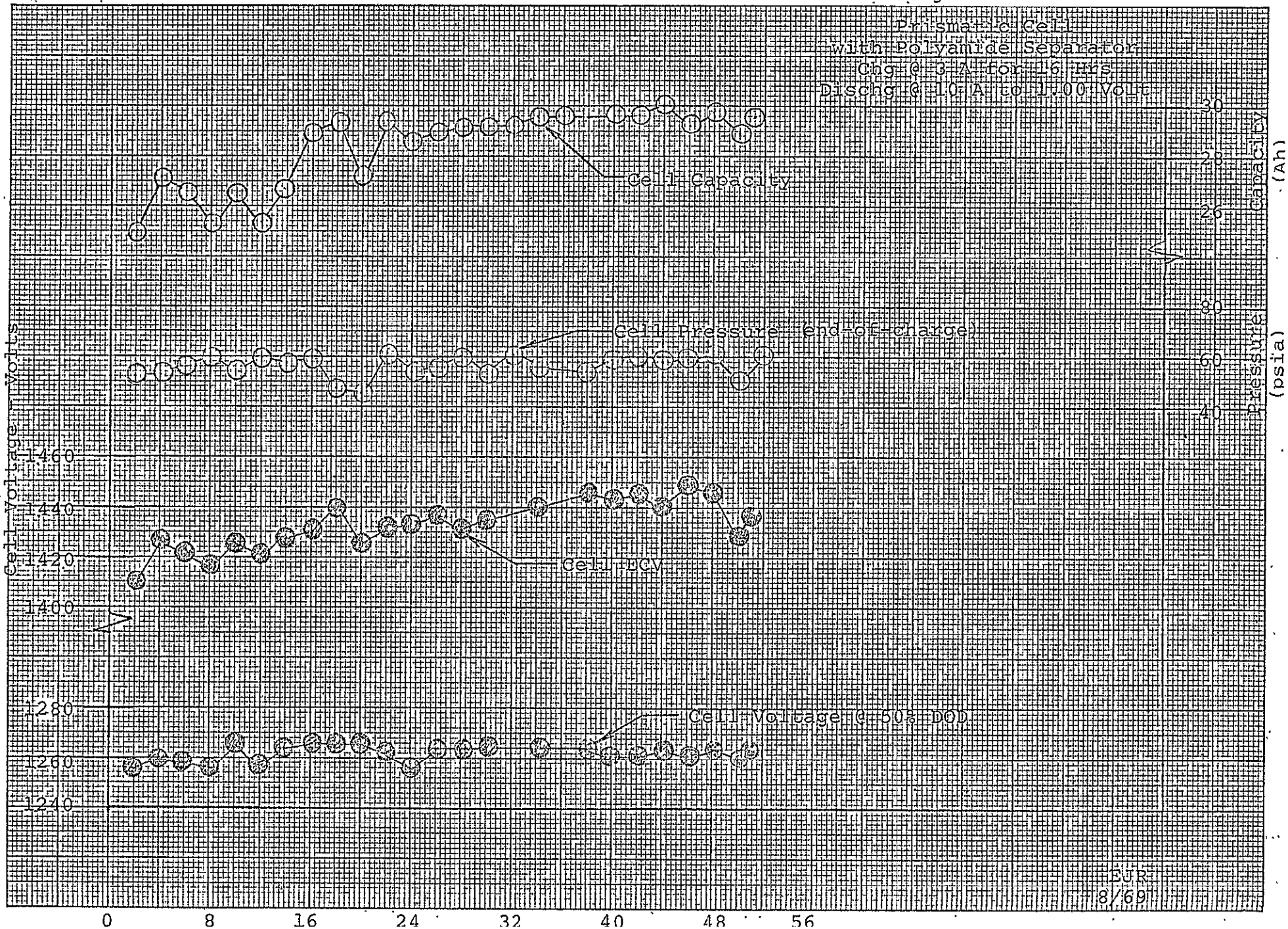

Based on the data of the previously reported cells and the mechanical designs discussed in the report for the seventh quarter, 1 January to 31 March, 1969, a group of 20 prismatic cells were built. The design characteristics are summarized in TABLE II-2.

TABLE II-2
Design Characteristics
25 Ah Heat Sterilizable
Prismatic Cells

Plates	
No. of positive	12
No. of negative	13
Ratio (Negative capacity to positive capacity)	1.4
Separator	FT2140
Electrolyte	
Quantity	78cc
Concentration	30%
Weight	1080 grams
Seals	Ceramic-to-metal

To date 10 of these cells have been characterized, heat sterilized and have undergone a single post heat sterilization cycle. These preliminary data correlate with the capacity and voltage behavior of the engineering development cells. The testing of these cells will continue to fifteen post sterilization. The remaining 10 cells will also be tested similarly after which these cells together with 20 cylindrical cells will be subjected to a long term testing program described in a subsequent section of this report.

C. Cylindrical Cells

The testing of cylindrical cells was conducted in a manner similar to the prismatic cells. These test data were used to generate final design data for heat sterilizable cylindrical cells.

The polyamide separator containing cell performance data is shown in Figure II-E. After 100 deep discharge cycles, the cell operating parameters remain stable. The variation in cell capacity during the first twenty five cycles are a result of fluctuations in test temperature and exceptions to the duty cycle described in the figure. The lower than normal (e.g. 1.25 v) middle-of-discharge voltage is a result of increased cell impedance caused by the previously reported tab arrangement and the out of roundness of the cell core. The specific energy exhibited by the cell is 14 to 14.5 watt-hours per pound. This value will be improved when the discharge voltage profile is increased.

The polypropylene separator containing non heat sterilized cell performance data is presented in Figure II-F. The lowered cell voltage at 50% is a result of increased cell impedance as previously described. The loss in cell capacity is not readily explained but may be an effect of the increased cell impedance. Cell pressure at the end-of-charge is also higher than cells with polyamide separator and is a result the lower recombination rate constant associated with polypropylene separators. Due to the lowered cell capacity and depressed discharge voltage the cell has a specific energy of 10 watt-hours per pound at the indicated duty cycle.

The heat sterilized polypropylene separator containing cell performance data is shown in Figure II-G. The cell reflects the effect of two changes in the cell design. Firstly the tab arrangement was changed to four 1/2 inch by .005 inch nickel tabs per plate. Also, the roundness of the cell core was improved which allows more even compression and therefore improved electrolyte distribution. Post sterilization behavior is characterized by increased end-of-charge voltage, an effect similar to that observed for prismatic cells.

Figure II-E

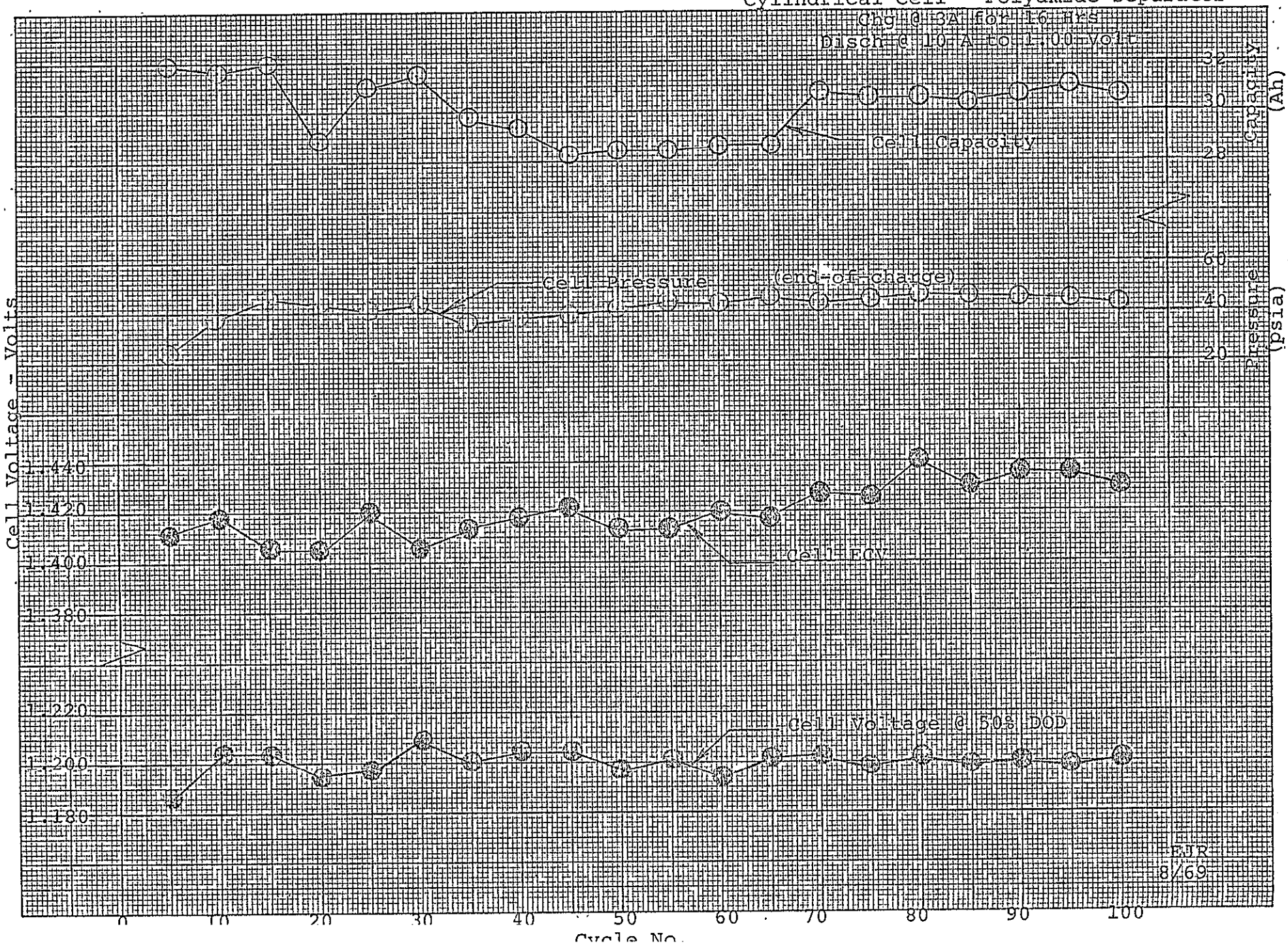

Figure II-E

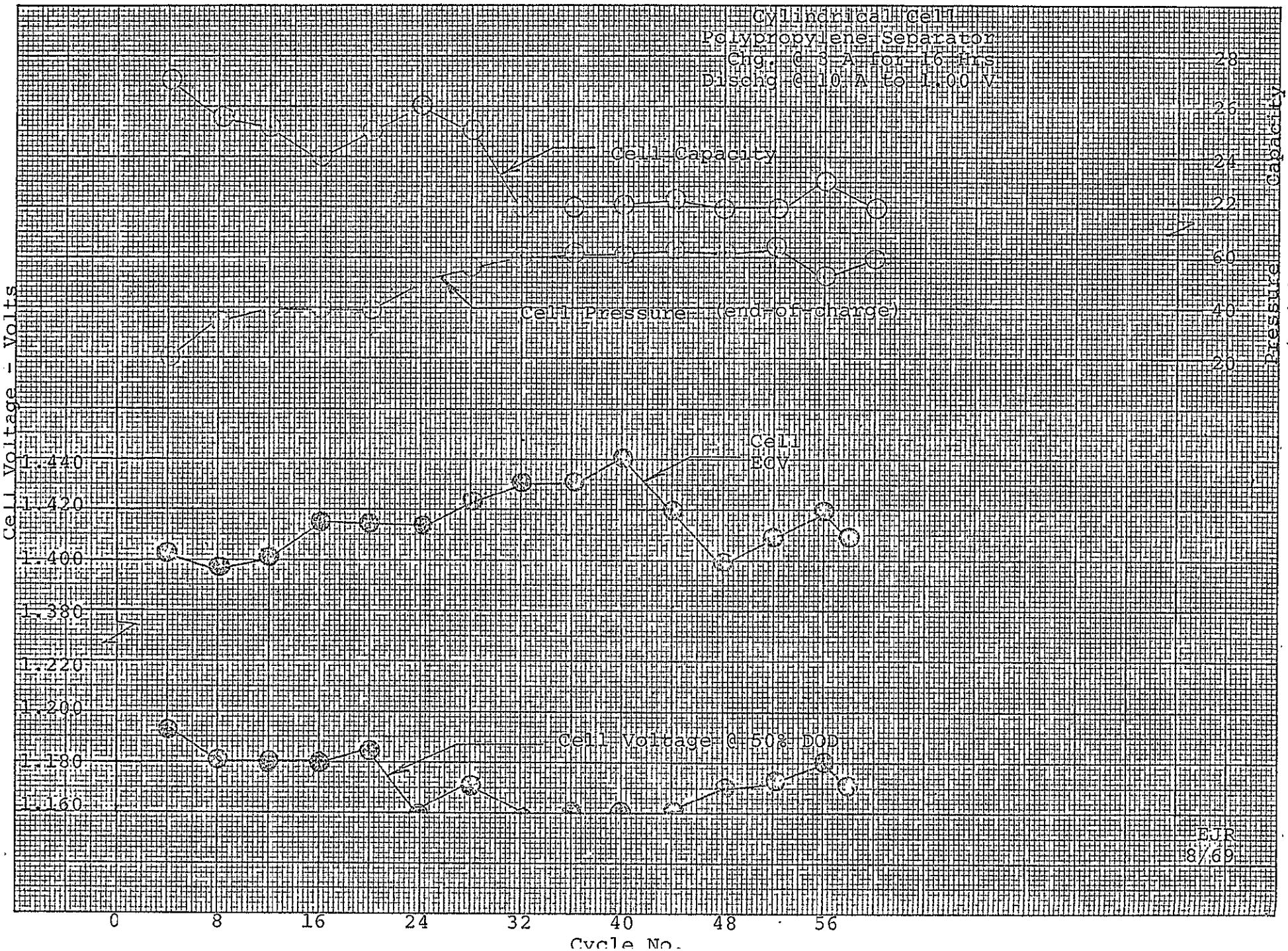

Figure-II-G

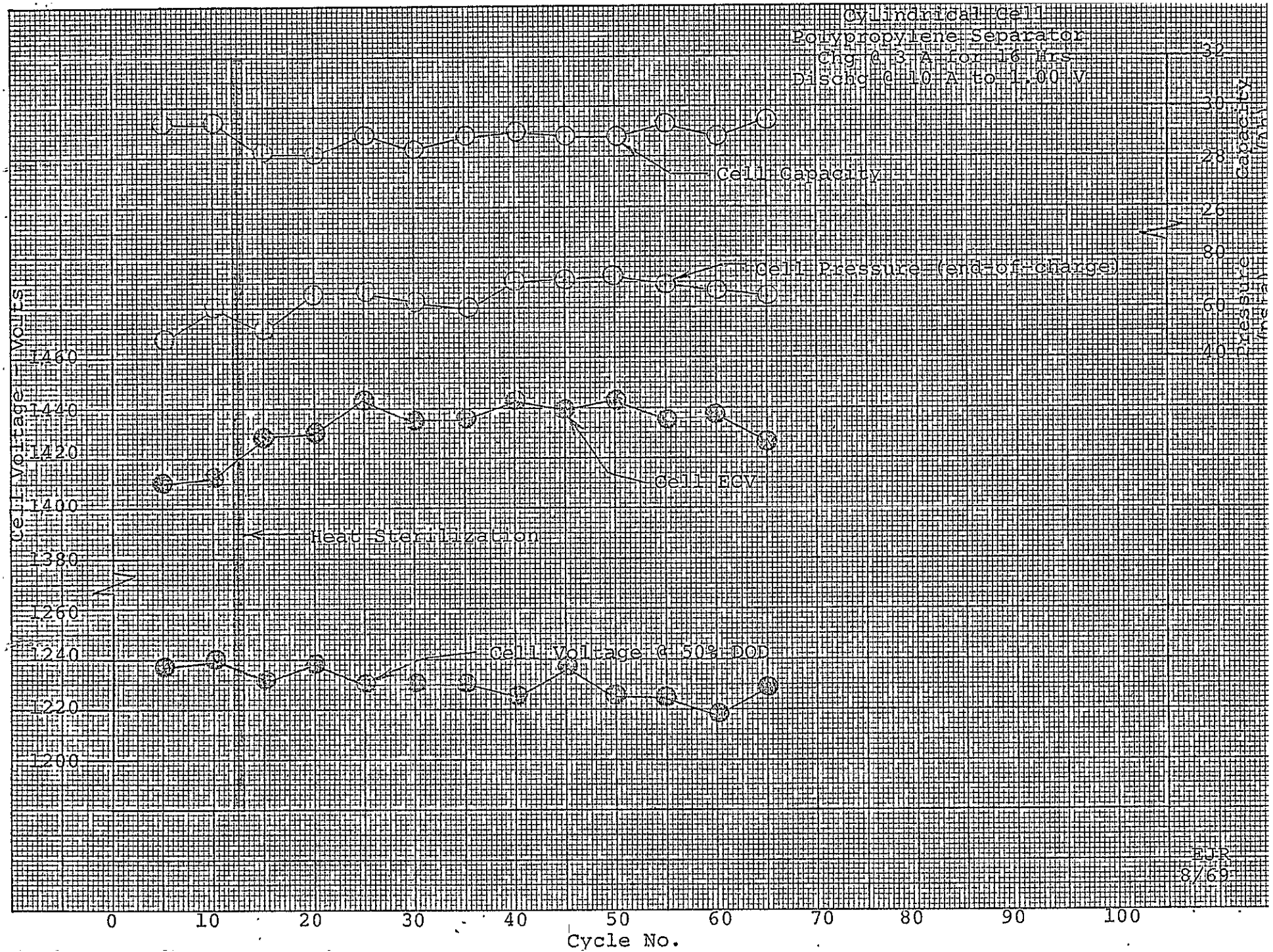

There are no other effects observed resulting from the heat sterilization process and the capacity has remained stable. The specific energy of this cell design is 14 watt-hours per pound.

Based on the data of the previously reported cells and the mechanical designs discussed in the report for the seventh quarter, 1 January to 31 March 1969, a group of 20 cylindrical cells were built. The design characteristics are summarized in TABLE II-3.

TABLE II-3
Design Characteristics
25 Ah Heat Sterilizable
Prismatic Cells

Plates	
No. of positive	3
No. of negative	4
Ratio (negative capacity to positive capacity)	1.65
Separator	FT2140
Electrolyte	
Quantity	90cc
Concentration	30%
Weight	1155 grams
Seals	glass-to-metal

To date 10 of these cells have been characterized, heat sterilized and have undergone a single post heat sterilization cycle. As with the prismatic cells, testing of these and the remaining 10 cells will continue and eventually be subjected to a long term testing program described next.

D. Long Term Testing Program

It is the purpose of this program to evaluate the proper storage methods (wet stand) and cycling conditions to allow power system designers to more accurately determine the capacity, durability and other physical and electrical parameters of

heat sterilizable nickel-cadmium systems. In addition, the data provided by this test program will allow for a proper selection of storage (wet stand) conditions consistant with mission requirements.

The proposed test conditions are outlined in TABLE II-4

TABLE II-4

A. Cycling - after heat sterilization and reconditioning

Test Termperature	30°F, 50°F, 70°F
Depth of Discharge	70%, 80%
Charge Rate	C/10, C/20
Discharge Rate	C/2
Cells Required	24 (12 prismatic, 12 cylindrical)
No. of Cycles	90 minimum, 150 planned

B. Cell Maintenance During Flight - after heat sterilization and reconditioning @70°F

Fly charged with periodic discharge and recharge - 2 cells
Fly discharged, charge at planet approach - 2 cells
Fly charged, trickle charge with constant current - 2 cells
Fly charged, float charge at constant voltage - 2 cells
Duration of wet stand shall be 7 months.

C. Cycling after Wet Stand

Cycle all cells for a minimum of 90 cycles under conditions optimized under Section A
Cell requirement for B & C is 8 cells each of prismatic and cylindrical design

Under part A the performance of cells under various duty cycles and temperatures will be determined. In a parallel test, the various charge maintenance regimes will be tested in part B to determine the optimum conditions for long stand times. These various conditions for wet stand were selected since they will effect the chemistry and morphology of the cell as previously described. The cells tested under part B will then be subjected to the cycling regime selected as optimum under part A of this testing program.

This testing sequence will provide data which is consistant with mission goals.

Cell parameters shown in TABLE II-5 will be measured and tabulated daily for the first 14 days of testing then at 7 day intervals throughout the testing program.

TABLE II-5

1.	end-of-charge voltage
2.	end-of-charge resistance
3.	end-of-charge pressure
4.	Cell capacity
5.	end-of-discharge voltage
6.	end-of-discharge resistance
7.	end-of-discharge pressure

All tests will be conducted in temperature controlled environmental chambers with accuracies of ±1°F. Charging and discharging will be performed using constant current power supplies except as noted in TABLE II-4.

Should any cell(s) fail during the testing program, the cause of the failure will be determined and documented.

The cells used for this program shall be the initial forty cells constructed under TASK X of JPL contract number 951972 to Texas Instruments. Twenty of these cells are of prismatic configuration and twenty of cylindrical configuration, both rated to deliver 25 ampere-hours at the C/2 rate after a 16 hour charge at the 10 hour rate. These cells will be characterized for parameters shown in TABLE II-5, as well as discharge profile (i.e. cell voltage at 25, 50, 75% depth-of-discharge prior to and after heat sterilization at 135°F for 72 hours). Prismatic cells will be constrained by plates during the testing period to prevent cell case distortion due to

internal pressures. Cylindrical cells will not be restrained.

E Continued Effort

Two other phases of the engineering development program are being conducted. The development of higher energy density plates has progressed beyond the point reported in the last quarter. To date the information developed from this study is being analyzed to determine which of these plate materials should be evaluated in the sealed and starved condition. Further progress will be reported in the next quarter.

The impact test data on the series of prismatic and cylindrical cells is completed. All X-rays and electrochemical testing have also been completed. These data will be correlated with the other physical testing and reported in the next quarterly report. The quantity of data generated has delayed completion of the reporting to date.

EIGHTH QTR JPL REPORT
April - June 1969
J. Gondusky

III. IMPACT TESTING SECTION

A. Development of high-impact testing facility.

B. Impact testing of existing Ni-Cd cells.
Figure III-A Table III-1

C. Testing of seals for Ni-Cd cells.
Table III-2

D. Testing of Ni-Cd electrodes.

1. Mechanical properties in tensile loading.

a. Constant deformation static testing.
Figure III-B Table III-3

b. Constant load static testing.
Figure III-C Table III-4

c. The effects of heat sterilization and electrolyte saturation. Table III-5

d. Dynamic tensile testing.
Figure III-D,E,F,G Table III-6,7

2. Mechanical properties in compression loading.

a. Introduction

b. Constant deformation static testing
Figure III-H Table III-8

c. Dynamic compression testing.
Figure III-I,J

3. Evaluation of strain-gage techniques.

a. Technique development
Figure III-K

b. Poisson's Ratio
Table III-9

LIST OF FIGURES

A. DEVELOPMENT OF HIGH-IMPACT TESTING FACILITY

The construction, development and calibration of our high-impact testing facility has been completely described in the seventh quarterly JPL report (Jan. - Mar. 1969). The facility has been extensively used during this quarter to evaluate battery electrodes and preliminary 25 AH cylindrical Ni-Cd cells. The operation and performance of this facility has been entirely satisfactory. However, we have made one rather important design or structural modification to the sliding carriage during this quarter which significantly improved the overall performance. The 8½" x 8½" x 2" thick aluminum main plate (best shown in Figure 4 of JPL 7th quarter report) has been replaced by a conical block of the same aluminum alloy. The shape is best described as a conical frustrum with a square base (8½" x 8½") and a circular top (4" dia.). The conical included angle is 80° providing a 6" height or "thickness" replacing the original 2" thick plate. This angle is the same as the tool angle and the 4" dia. top matches the tool's base exactly. Thus we have a smoother transition from tool to specimen mounting and have essentially eliminated the vibration problems that existed as previously discussed. Because of the increased weight and associated momentum, tools of larger diameters were required to maintain the upper g-levels. However, the resultant shift in calibration is fully compensated by the increased structural rigidity and the resultant improvement of system performance.

B. IMPACT TESTING OF EXISTING Ni-Cd CELLS

As indicated in the March Monthly Report, all programmed impact testing of existing cells has been completed. Although, the post-impact x-ray and electrochemical characterization work is now underway, it will be some time before a complete analysis is available. As an interim measure, it may be appropriate to report the impact observations in advance. True "failure" may be electrochemically defined later as the cell's inability to deliver suitable discharge capacity following an impact environment. At present, it is necessary to establish another interim failure criterion. Since we have monitored a cell's open circuit voltage during impact, we can use this as an indicator of electrical damage. Typical of the information provided by this failure indicator are the phenomenon shown in Figure III-A. The upper trace displays the cell's open circuit voltage from 5 msec. before impact to 15 msec. after impact. The three oscillographs presented indicate the classifications of impact - induced damage:

(a)	no cell damage	(N)	$V_2=V_1$	no ΔV @ impact
(b)	questionable damage	(P)	$V_2=V_1$	ΔV @ impact (momemtary shorting)
(c)	failure	(F)	$V_2<V_1$	ΔV @ impact (complete shorting or loss of plates

The type of behavior exhibited in (b) is of very questionable damage electrochemically. We assume that such a momentary short will have little effect on the following discharge capacity and certainly not prevent the cell from subsequent cycling. However, until this is confirmed by our post - impact characterization, we will distinguish this observed behavior from that of a complete satisfactory performance.

The total study of existing cells involved 52 impact tests to evaluate the performance of four (4) types of Ni-Cd cells:

(1) C Sub-C without spindle (part #006200)
(2) CS Sub-C with spindle (part #003800)
(3) LC Long Sub-C without spindle (part #005500)
(4) P Prismatic 4 A.H. (part #003500)

Each type of cell was tested in each non-redundant direction at three average impact levels: 2300g, 2960g, 3950g

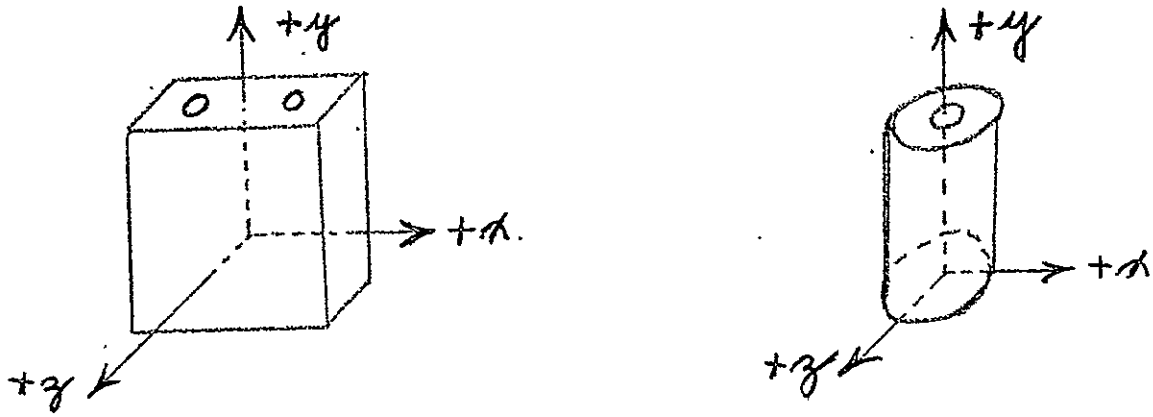

NOTE: Impact in +y direction implies:

$\vec{v}$ in +y direction
$\vec{a}$ in -y direction
impact surface -- terminal end (+y)

UPPER BEAM:

OC VOLTAGE OF CELL
VERT: 1 VOLT/CM
HORIZ: 2 msec/CM

LOWER BEAM:

ACCELERATION
VERT: 1000g/CM
HORIZ: 0.5 msec/CM

a)

NO CELL DAMAGE

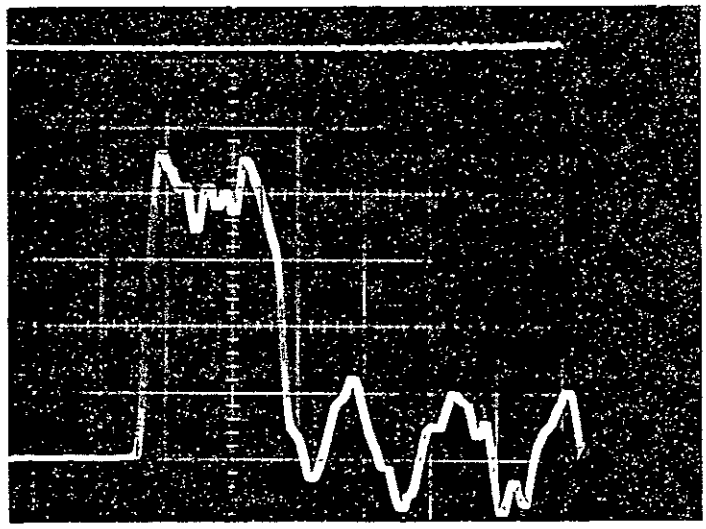

b)

MOMENTARY
SHORTING
DURING IMPACT

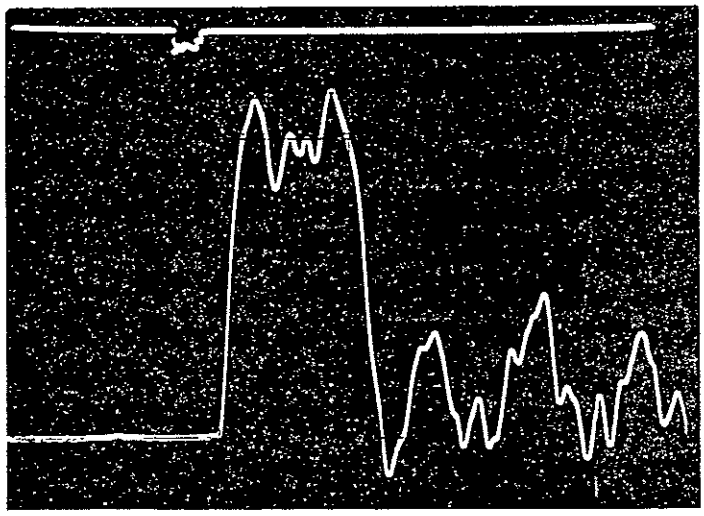

c)

COMPLETE
CELL FAILURE
AT IMPACT

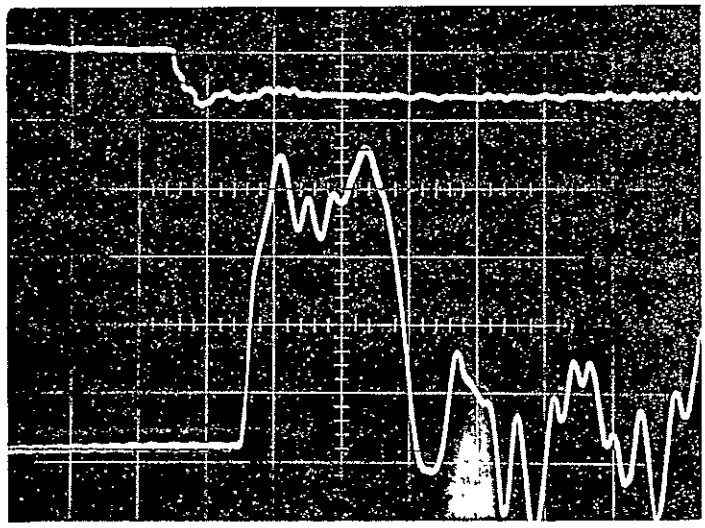

Fig. III A

Table III-1 summarizes the results of the complete study. Each type of cell is shown with the directions of impact included. The actual impact (meas. mean g-level and velocity) is stated and the observed cell behavior. It must be emphasized that none of these cells were designed specifically for impact-resistance. The inherent impact resistance exhibited (or the lack of it) is not meant to imply the actual shock resistance that can be attained by any of the configurations that have been studied. The obvious example is the prismatic cell where great gains could be expected for the $\pm y$ direction with a minimum of design improvement.

In general, we have been encouraged by the preliminary analysis of this study. The cylindrical cells have performed quite well, however, subtleties exist that must await the x-ray and post-mortem observations before we can fully understand the cells' behavior. For example, the Sub-C with spindle seems to have more potential damage in the x direction than the same cell configuration without a spindle. The long Sub-C seems to have experienced more difficulty in the -y direction than in the +y direction. Similarly, the prismatic results in the $\pm y$ directions were anticipated, but there are questions concerning the reason for poor behavior in the z direction at the highest impact level. It is not the scope of this interim report to account for these details. A more accurate report of the failure modes will accompany the final report which will include complete x-ray and electrochemical performance information.

TABLE III-1

Cell Type & Impact Direction		Low Impact Level (g)	(V) ft/sec.	Beha-vior	Med. Impact Level (g)	(V)	Beha-vior	High Impact Level (g)	(V)	Beha-vior
Sub-C	x	2000	(87)	N	2800	(106)	N	3800	(118)	N
Without	-y	2350	(86)	N	2700	(107)	N	4170	(122)	P
								4100	(113)	N
Spindle	+y	2350	(--)	N	3400	(102)	N	3500	(120)	P
								4200	(115)	N
Sub-C	x	2000	(88)	N	3400	(106)	N	3600	(122)	F
								3600	(123)	P
With	-y	2520	(89)	N	2750	(106)	P	4600	(121)	P
		2050	(86)	N						
Spindle	+y	2400	(87)	N	2800	(108)	P	4800	(119)	N
Long	z	2100	(89)	N	2700	(107)	N	3500	(122)	N
Sub-C	x	2350	(88)	N	3400	(106)	N	3500	(121)	N
Without	-y	2450	(86)	P	3120	(105)	P	3700	(119)	P
					3000	(105)	P			
Spindle	+y	2300	(90)	N	2700	(106)	N	3700	(117)	P
								4600	(116)	P
Prismatic	z	2250	(89)	N	2500	(104)	N	4070	(114)	P
								4020	(111)	P
4 A.H.								3800	(120)	F
	x	2300	(89)	N	2850	(105)	P	4400	(120)	P
	-y	2300	(88)	F	2800	(104)	F	3100	(112)	F
	+y	2600	(87)	F	3200	(102)	F	3800	(113)	F

CELL BEHAVIOR CODE: N - no damage
P - possible damage
F - failure

TESTING OF HIGH-CAPACITY CELLS

In addition to the programmed testing of smaller production cells, two 25 AH cylindrical prototype cells have been tested. It must be emphasized that neither cell was heat-sterilizable and more importantly, not designed for impact resistance. The tests were meant solely to study the mounting techniques and practical aspects that might occur with the larger cells.

The first test was conducted at 3400 g (4000g CALC.) from 119.5 ft/sec. with the cell mounted transversly (x-z direction) on a rigid half-space. During acceleration the hold down strap severly dented the cell case, yet the cell voltage trace during impact indicated a complete lack of electrical damage. This cell had been partially discharged before impact and following impact it delivered the full remainder of capacity as determined from previous cycling data on this cell. X-ray analysis of the cell indicated large deformation yet complete integrity of the cell components.

The second test was conducted at 3600 g (4250 g CALC.) from 116.5 ft/sec. with the cell experiencing axial impact against the bottom (-y direction). The cell voltage trace indicated a complete shorting of the cell during acceleration. Subsequent x-ray analysis showed the deformations responsible for this shorting as well as those associated with the main decelleration at impact. A post-mortem investigation revealed the short location beneath the negative terminal which had punctured the thin separator during pack movement toward the terminal end (+y) of the cell. Without the benefit of a suitable spacer to prevent initial axial pack motion, this result is rather obvious. The main impact decelleration is of course highly amplified because of this initial motion and little true information can be inferred.

This testing did indicate however, that there were few difficulties in testing the higher capacity cells.

C. TESTING OF SEALS FOR Ni-Cd CELLS

The complete seal evaluation program as outlined in the 7th QTR JPL report has been delayed by the inavailability of seals. This postponement does not affect the overall impact testing program. However, during April we felt it was desirable to obtain a preliminary indication of the ceramic-to-metal seal's strength, since this type of seal is on hand and has been suggested as a possible alternative design on impact-resistant cells. The static loading (before heat-sterilization) portion of the overall evaluation program was thus performed on 3 types of ceramic-to-metal seals. Fixtures were employed which held the outer metal flange of the seal rigid and allowed the load to be applied through the pin either in compression or tension.

The loading information and description of the seals is contained in Table III-2. It was found that tensile tests for this type of small pin diameter (conductor) will yield no meaningful information except a very lower bound on the static strength of the ceramic element and the ceramic-braze-flange joint. In compression, all loads were associated with flange failure, which is both interesting and encouraging, since it implies that both the ceramic element and the ceramic-pin interface are quite strong.

TABLE III-2

Seal Type	Type Load	Rate of Loading (in/min.)	Load (#)	Failure Mode
Ceramaseal #800A0200-1	Tension	2.0	300	Pin Fracture
1/8" dia. Copper Pin	Comp.	2.0	1220	Flange-Braze Shear
42% Ni-Fe Flange	"	0.2	1150	Flange Shear
92% Alumina				
Total Wt. 4.7 gm.				
Ceramaseal #800A0205-1	Tension	2.0	230	Pin Fracture
1/16" dia. Kovar Pin				
42% Ni-Fe Flange	Comp.	2.0	370	Bending Pin
92% Alumina				
Total Wt. 1.0 gm.	"	0.2	550	Flange Shear
Ceramaseal #800A0208-1	Tension	2.0	440	Pin Fracture
3/32" dia. Kovar Pin				
42% Ni-Fe Flange	Comp.	2.0	175	Bending Flange Tearing Braze-Ceramic Interface
92% Alumina	"	0.2	180	" "
Total Wt. 2.3 gm. (wide Flange)				

In fact, these load values are quite high and using the entire mass of the seal, would imply dynamic resistance on the order of 10^5g. We were unable to observe any effect from the rate of loading which is not surprising, since both values are essentially static when compared to real impact conditions. There is little basis at this point to make a valid prediction concerning the g-level that could be survived by these seals. However, indications are than these seals alone should have little difficulty withstanding 4000g levels of impact. The amount of extra mass (tabs, combs, nuts, etc.) that could be safely added to the center conducting pin remains a question that will be answered during actual impact testing. Since extraneous mass could be easily de-coupled if found necessary, additional testing will not proceed immediately beyond this initial phase that has been reported. We are satisfied with this preliminary information. Further impact testing is postponed until crimp-polymeric seals and stainless steel headers for the ceramic-to-metal seals become available.

D. TESTING OF Ni-Cd ELECTRODES

1. MECHANICAL PROPERTIES IN TENSILE LOADING

a. Constant Deformation Static Testing

The initial studies of the mechanical properties of Ni-Cd electrodes involved the static determination of "conventional" stress-strain curves in tension. "Conventional" here means the engineering σ-ϵ curve as established by constant deformation loading. All test samples consisted of 1/2" wide x 6" long strips containing exactly ten (10) longitudinal screen wires. An Instron commercial testing machine was used with a cross head speed of 0.1 in./min. over a 4" initial gage length for a constant strain rate, $\dot{\epsilon}$, equal to 0.0004" sec^{-1}. With cross head speed related to chart speed, the x-axis as deformation was established and with load cell output on the y-axis we received initial data in the form of a direct load vs. deformation plot which was then easily converted to a stress-strain curve. For positive plate, negative plate, positive plaque and negative plaque the stress is simply the load divided by the actual measured area of the specimen (typically positive plate 0.500" wide x .026" thick = .013 $in.^2$). However, for screen specimens, an arbitrary apparent area of 0.013 $in.^2$ was taken to permit strength comparisons with the final plate material (i.e. how much apparent stress in a positive plate is actually supported by the screen wires alone?). Strain of course was determined simply from the deformation divided by the initial 4 inch gage length. Hence, what we sought from this type of testing was the comparative strengths of the screen alone, the reinforcement associated with the sintered nickel matrix and finally the actual strengths and differences in strength of positive and negative plate. Thus, the rough determination of modulus of elasticity, the engineering yield strength (0.2% ϵ), the ultimate strength, elongation (% in 4" G.L.) and most importantly, the complete shape of the stress-strain curve into the plastic region were of immediate concern. Several specimens were tested of each of the five "materials" of interest.

Reproducibility is excellent in this type of loading and the average results for each material are shown tabulated below with respect to important values describing the mechanical behavior.

TABLE III-3

	ANNEALED SCREEN	NEGATIVE PLAQUE (905)	POSITIVE PLAQUE (810)	NEGATIVE PLATE (170)	POSITIVE PLATE (176)
E (PSI)	0.18×10^6	0.23×10^6	0.47×10^6	0.41×10^6	0.58×10^6
P_{yield} (LBS)	2.9	5.1	11.1	10.0	11.05
σ_{yield} (PSI)	225	390	855	710	850
P_{ult} (LBS)	16.8	17.3	18.9	19.1	18.1
σ_{ult} (PSI)	1290	1330	1450	1360	1390
Elongation (%)	20.7	22.8	17.7	18.5	20.5

* Dry, as manufactured electrodes

In order to summarize the results of this study more clearly, Figure III-B has been prepared to show the average stress-strain curve obtained for each material studied. The curve for screen alone essentially lays the foundation of comparison in this study.

We can observe the progression of increased strength from the basic screen grid through negative plaque, negative plate, positive plate and finally positive plaque. It is desirable to compare these various materials with regard to three important quantities:

(1) Modulus of Elasticity

The values for each material were tabulated as an indication of

FIG III B

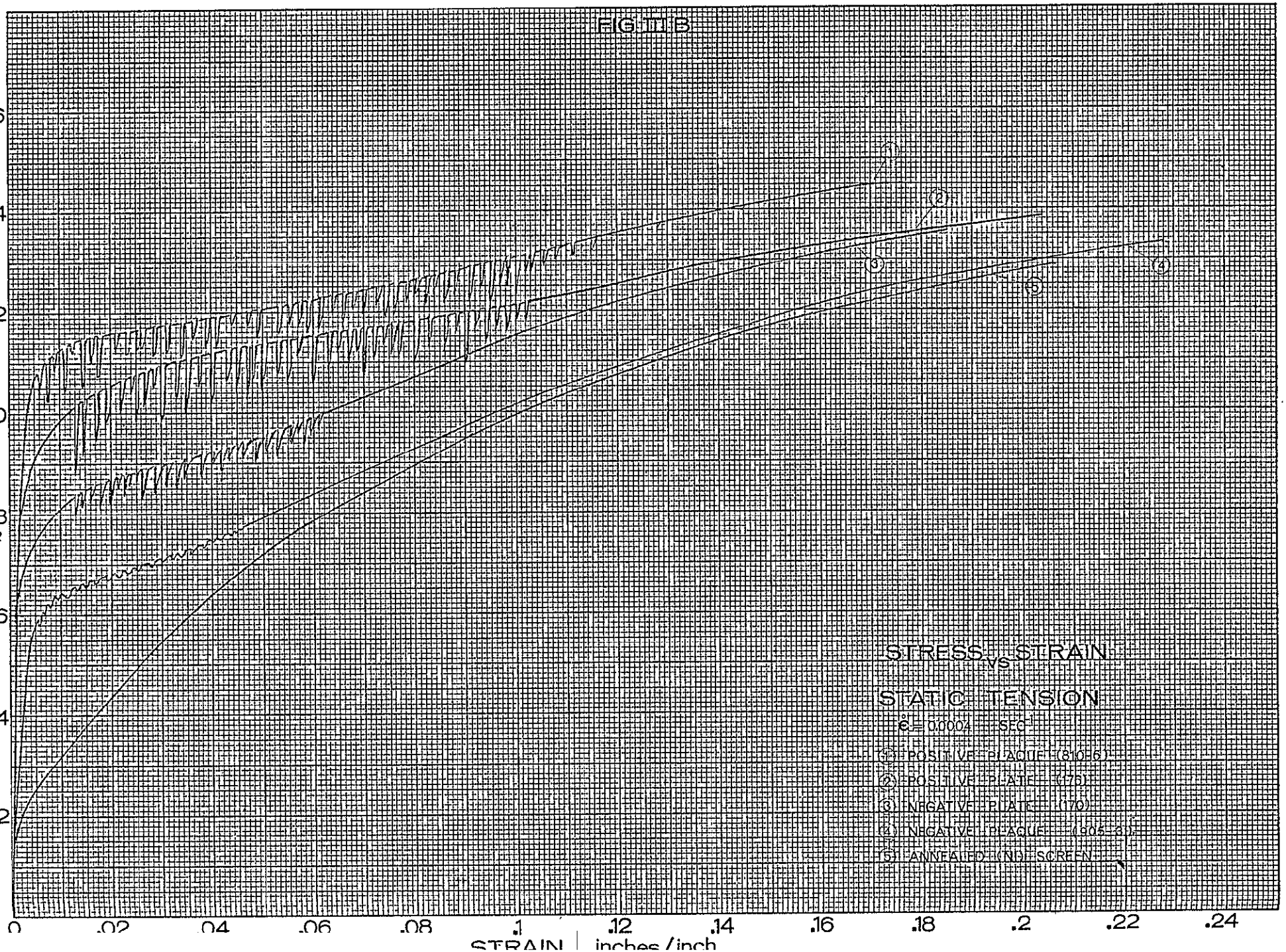

relative strength. They were determined from approximate slopes of the initial portion of the σ-ε curves. They are valid as a confirmation of relative strength but tend to be low in absolute value. Section D1b of this report describes in greater detail the results obtained from a more precise method of determining this quantity.

(2) Yield Strength

The prime consideration in discussing yield strength is the degree of basic grid reinforcement that is attributable to the addition of the matrix. As first applied to the basic grid, this matrix of sintered Ni powder forms plaque. The first important result of this study was the significant difference in strength between positive and negative plaque. Positive plaque has a much higher yield strength than negative plaque. Although both materials are manufactured from the same slurry formulation and have the same thickness (.026"), the positive has a higher area density than the negative (0.6 gm sinter/in.^{2} vs. 0.5 gm sinter/in.^{2}). The positive plaque has less total porosity than the negative plaque (79.5% vs. 83.6%) and in addition the sintering temperature is higher for positive plaque than for negative plaque (1980°F. vs. 1700°F.). These facts explain very readily the reason for the increased strength of positive plaque.

The next significant effect shown is the reduction in strength that occurs when positive plaque is electrochemically formed into positive plate. Porosity alone is certainly no indication of this effect for it is not uncommon to reduce the total porosity to 33%. The factor that is important is the 30% wt. corrosion of the sinter matrix which occurs during the process. It is true that positive active material ($Ni(OH)_2$/NiOOH) is deposited within the pores and results in the lowered porosity, but it appears that this material in hydroxide compound form adds little

strength to the material. The overiding effect then, is the significant weakening of the initially strong positive plaque matrix by the extensive corrosion associated with impregnation.

Equally significant is the reverse strength effect we have observed associated with the manufacture of negative plate. Negative plate material has a higher yield strength than the initial negative plaque. The total porosity is decreased to 56% during this process but again, it is the manner in which this change occurs that is important. Corrosion (20-25% wt.) of the sinter matrix also occurs during the electrochemical formation of negative plate and likewise the impregnation with active material takes place.

Firstly however, the amount of sintered matrix corrosion is less for the negative plate than for the positive plate. Secondly, the neg. active mat. ($Cd/Cd(OH)_2$) partially as a metal, has more strength than the positive compounds. It is, therefore, apparent that the lower amount of corrosion combined with the overiding factor of a stronger active material produce the net strengthening of negative plate. It is shown as a final result that positive plate material has a higher yield strength than negative plate material. This is obvious at the 0.2% ε point, by the higher modulus of elasticity, and by the larger drop of load as the matrix cracks. The last indicator is a result of the constant $\dot{\varepsilon}$ loading employed. (Viz., as each matrix crack forms, a drop in the load being carried across that section is exhibited on the σ-ε curve) it is significant to note then that not only is the positive plate matrix stronger, but that it continues to help support load further into the high strain region. It seems then, that even after considering the differences in corrosion and impregnation phenomenon, the positive Ni plate is stronger than the negative Cd plate primarily because there is such a great

difference in their respective parent structures - the positive and negative sinter material - plaque.

(3) Ultimate Strength

Although the basic progressive ineffectiveness of the matrix has been shown by the reversion of plaque/plate strength to that of screen alone, it is first important to note that the ultimate strength of all four matrix materials remains slightly higher than that of screen alone. This may be accounted for by assuming that some of the nickel powder has been effectively sintered to the screen wires or in the immediate vicinity and permits this small portion of the matrix to provide continued reinforcement throughout elongation to fracture. If this is indeed the mechanism acting, we can then also explain the relative values of ultimate strength from the corrosion consideration discussed earlier. Firstly, it is reasonable to expect the higher density, higher temperature sinter of the positive plaque to exhibit the highest ultimate stress which indeed is the case. Secondly, we note that dispite a stronger matrix at yield, the positive plate has a lower ultimate strength (absolute load) than the negative. Here the greater corrosion of the positive wires and proximate matrix would tend to weaken and lower the ultimate strength below that of the negative plate. It might be noted that as the screen strength begins to dominate at the higher strain levels, stress values become less important than absolute loads. Although the differences are not great, they do provide insight as to the mechanisms that may be involved.

b. Constant Load Static Testing

Although the previous study is an excellent starting point for an investigation of a material's mechanical behavior and provides the usual engineering understanding, it may not provide the optimum information for our purposes. In other words, under impact conditions, a constant acceleration field is created to act upon the mass of the structural element in question. This constant inertia loading is not exactly equivalent to the type of constant deformation loading used in the previous study. It was also desirable to expand the area of low strain (<1%) to more accurately determine the modulus of elasticity and examine the yield phenomena more closely. Thus, we employed a constant load test frame rather than the commercial constant deformation type used in the preliminary studies. This arrangement applied load to the specimen by means of a water fill technique. A container attached to the specimen served as a dead weight accumulator as it was filled with water at a constant rate. The rate of loading is selected by the operator before each test via a constant head supply and solenoid control valves. Additionally, unloading at any point along the stress-strain curve is easily accomplished at a fairly uniform rate by draining water from the accumulator. Load is measured by a strain gage proof ring and the signal plotted directly on the vertical axis of an x-y recorder. Strain measurements are taken more accurately by a strain gage extensometer of 1" gage length mounted on the specimen. This output is plotted directly on the horizontal axis of the x-y recorder. This system provided a very deliberate manner of loading to closely examine the region of yielding. Especially because of our ability to unload very precisely, we were also able to examine the modulus of elasticity of the material and its relation to strain level. Again, the average results for each material are shown in Table III-4 with respect to the important values describing its mechanical behavior.

TABLE III-4

	ANNEALED SCREEN	* NEGATIVE PLATE	* POSITIVE PLATE
E (PSI)	$0.8 \pm 0.2 \times 10^6$	$1.0 \pm 0.1 \times 10^6$	$1.2 \pm 0.2 \times 10^6$
P_{yield} (LBS)	3.1	9.9	11.2
σ_{yield} (PSI)	240	705	860
P_{ult} (LBS)	17.0	19.8	19.1
σ_{ult} (PSI)	1310	1420	1470

* Dry, as manufactured electrodes

Figure III- C has been prepared to permit comparison of the average stress-strain curve associated with each material studied. It is shown once again that the screen alone forms the foundation and the increased strength due to the matrix is very obvious in this region of low strain (<1%.). The tabulated values of strength agree quite well with those obtained under the constant deformation type of loading. However, this description of strength was obtained in a different manner and it is best to consider each value separately.

(1) Modulus of Elasticity

As the matrix becomes ineffective, (while cracks form as strain level progresses), we would expect to see a progressive decrease in the initial modulus value toward the lower value of screen alone. As indicated, the constant load technique allows us to unload and reload at any strain level we chose to determine the elastic modulus at that strain level. In practive, we were able to unload and reload at 400 μin./in. $< \varepsilon <$ 6000 μin./in. Within this region, the experimental scatter is equal to the diminishing

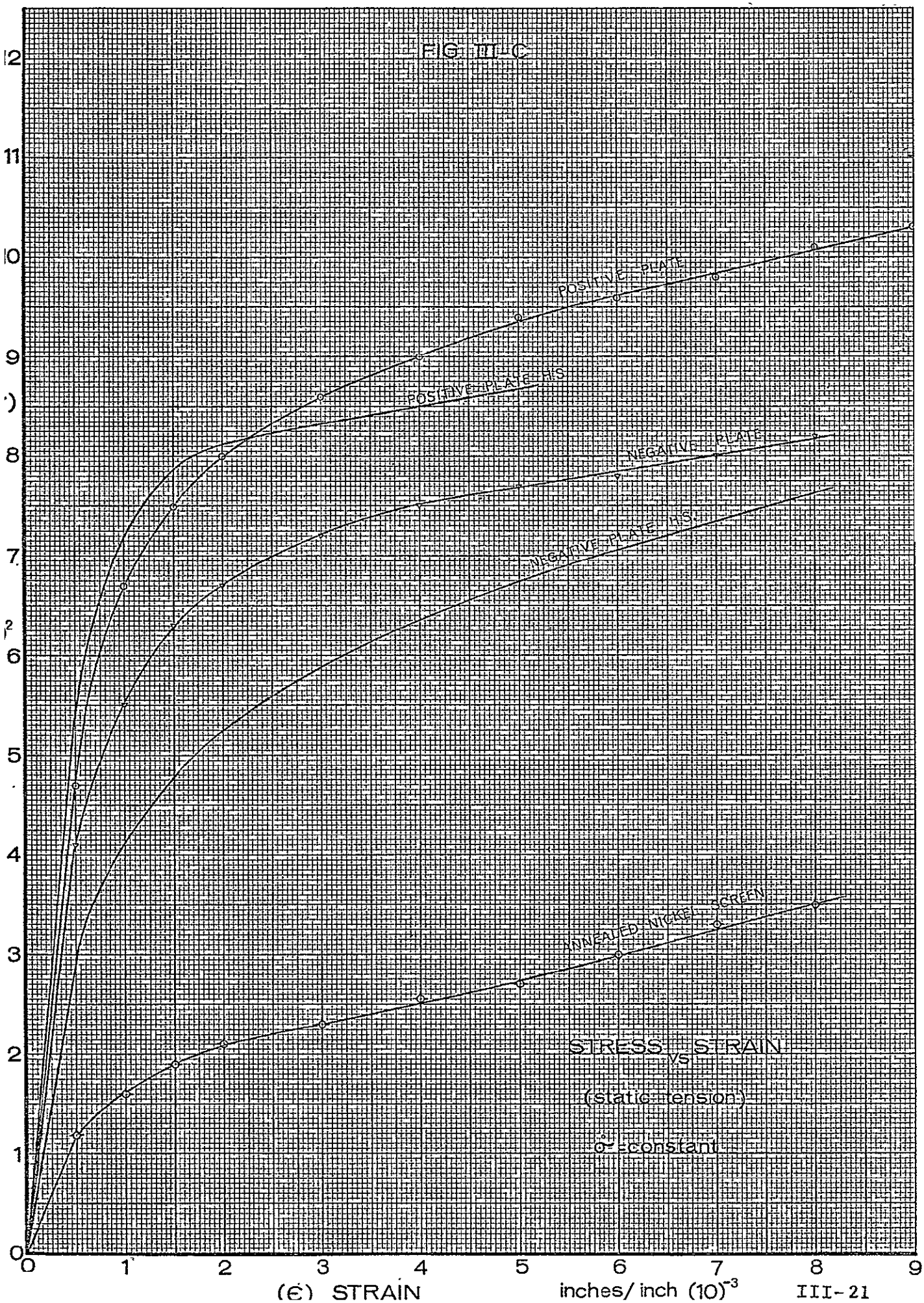

function which may exist. Some values were obtained near the 200$\mu\varepsilon$ level and they were higher than the average reported. The values that have been given in Table III-4 are the average values obtained from all unload-reload determinations within 400μ in./in. $<\varepsilon<$ 6000μ in./in. for each material. The tolerance is that of experimental error combined with any diminishing function that may exist within this region of strain. We have of course, plotted E vs. ε for each material and can only say that three regions of interest seem to exist: (a) E may be diminished rapidly in the region $0<\varepsilon<$ 200μ in./in. (b) for the region 200μ in./in. $<\varepsilon<$ 2000μ in./in. there may exist a very small diminishing of E. (c) beyond ε = 2000μ in./in. there seems to be no function of E vs. ε level. In other words we feel that a plastic deformation component exists at very low strain levels (<200μ in./in.) and that yielding is complete @ 2000$\mu\varepsilon$. This is confirmed by the fact that a determination of modulus of elasticity by measuring the slope of the stress strain curves (as done for Table III-3.) shown in Figure III-B and III-C will give a lower value than that obtained by the more accurate unload-reload technique. The values indicated in Table III-4, therefore, remain the best measure of true elastic responce in tensile loading. Aside from permitting future calculations of dynamic response, they are important measurements for several reasons: (a) the value obtained for screen alone agrees well with that indicated in the previous model discussion (7th JPL QTR Report). (b) at least for $\varepsilon<$ 6000μ in./in. the modulus of plate material remains higher than that of screen alone (yet not as high as the model predicted). (c) the strength (stiffness) of the positive matrix is greater than that of the negative matrix. This was first suggested by the differences in the deformation pattern observed for positive vs. negative plates (i.e. longitudinal as well as transverse matrix cracks were formed only in the negative).

(2) Yield Strength

As indicated, this type of precise loading was meant to more accurately examine the region of yielding $\varepsilon<1\%$. Figure III-C illustrates this region in great detail. It is important only to note that this value of yield strength @ 0.2% ε agrees very well with the initial determination given in Table III-3. Thus, this series of constant load tests fully supports the initial relations between positive and negative plates as extensively discussed in the previous section.

(3) Ultimate Strength

Although this type of testing was meant to closely examine only the low strain region near yielding, most specimens were taken to tensile fracture. Load data was available up to the point of failure and it is important only to note that the ultimate strengths thus reported are essentially in agreement with those first determined and reported in Table III-3. Thus, this series of constant load tests essentially supports the discussion of ultimate strength contained in the earlier section.

C. THE EFFECTS OF HEAT STERILIZATION AND ELECTROLYTE SATURATION

All tabulated values and stress-strain curves shown in the preceding sections were obtained from as-manufactured, dry, unsterilized plate material. We were interested, therefore, in the possible changes in mechanical properties which might result from heat sterilization and electrolyte saturation of this same plate material. Tensile samples were thus prepared by full heat sterilization (135°C for 64 hours) in the saturated condition (30% KOH). These specimens were then tested in the constant loading apparatus described in section D1b The results are tabulated below and should be compared to those in Table III-4.

TABLE III- 5

SATURATED AND STERILIZED ELECTRODES

E (psi)	Negative Plate $0.71 \pm 0.10 \times 10^6$	Positive Plate $1.35 \pm 0.25 \times 10^6$
P_{yield} (lb)	8.2	10.9
σ_{yield} (psi)	587	835
P_{ult} (lb)	19.2	22.0
σ_{ult} (psi)	1375	1690

The complete stress-strain curves have also been included in Fig. III-C in order to permit the comparison of as-manufactured vs saturated and heat-sterilized plates.

It appears that the mechanical properties of the positive plate material are not changed as greatly as those of the negative plate.

The positive results indicate very small changes in the modulus of elasticity and yield strength. However, the ultimate strength has been found to be significantly higher and, since this is essentially determined by the screen wires, we might assume that this is the result of a metallurgical change; viz, an embrittlement of nickel metal as a result of sustained exposure to hot KOH. Yet this is not clear since negative results do not concur.

The behavior of negative plate is changed a great deal by this saturated sterilization. It is interesting to note that we had reported (2nd JPL Quarterly) porosity changes for dry plates, before and after heat sterilization, as follows:

Pos. as-manuf.	33.4%	→	Pos. ster.	45.2%
Neg. as-manuf.	55.9%	→	Neg. ster.	55.5%

This might predict greater changes for the positive than the negative and we have found the exact opposite. The modulus of elasticity and yield strength of the negative has been significantly lowered along with a slight reduction in ultimate strength. Experimentally, we did not separate the effects of heat sterilization (dry) from those of electrolyte saturation and therefore cannot give an accurate account of the causes for the observed behavior. We may wish to study this area further, particularly if we find substantial effects under compressive loads. At this time we can only note that from a strength, and thus impact resistant, point of view the weaker of the two electrodes in our

Ni-Cd system seems to be further weakened by the saturated sterilization treatment that may be required.

d. DYNAMIC TENSILE TESTING

Considering the goal of the current effort to develop knowledge which will enable the design of impact resistant Ni-Cd cells, it should be stated that the actual dynamic tests are of prime importance. In retrospect to what has been written, it should be stated that the reason for performing static testing is to establish a foundation of strength properties. What is necessary for a thorough understanding is a knowledge of the actual transfer from static to dynamic conditions. The static testing is valuable since it can provide us with a complete picture of stress vs strain which is not easily obtained under dynamic loading. In fact, it will be shown that only the yield point and ultimate load can be obtained under dynamic conditions and that the static results are of great value in establishing the complete mechanical behavior.

(1) Ultimate Strength

By way of illustration, it is appropriate to review the initial considerations which preceded the commencement of dynamic testing. The essential question might well be asked, "What is the maximum length that a positive plate can be and yet avoid ultimate tensile failure while experiencing a shock environment of 4000g?" From the static values we have obtained and a knowledge of the plate's physical properties, we might write

$$\left(\frac{\text{Ultimate Force}}{\text{Unit Width}}\right) = \left[\frac{(\text{Length})\left(\frac{\text{Unit}}{\text{Width}}\right)\left(\frac{\text{Area}}{\text{Density}}\right)}{g}\right](N\ g)$$

and would find that

$$\ell \geq 3.3 \text{ inch} \Rightarrow \text{Failure}$$

This mass, inertia-loading approach defines the method of testing we have used to investigate dynamic tensile properties. The essential concept is shown diagrammatically below.

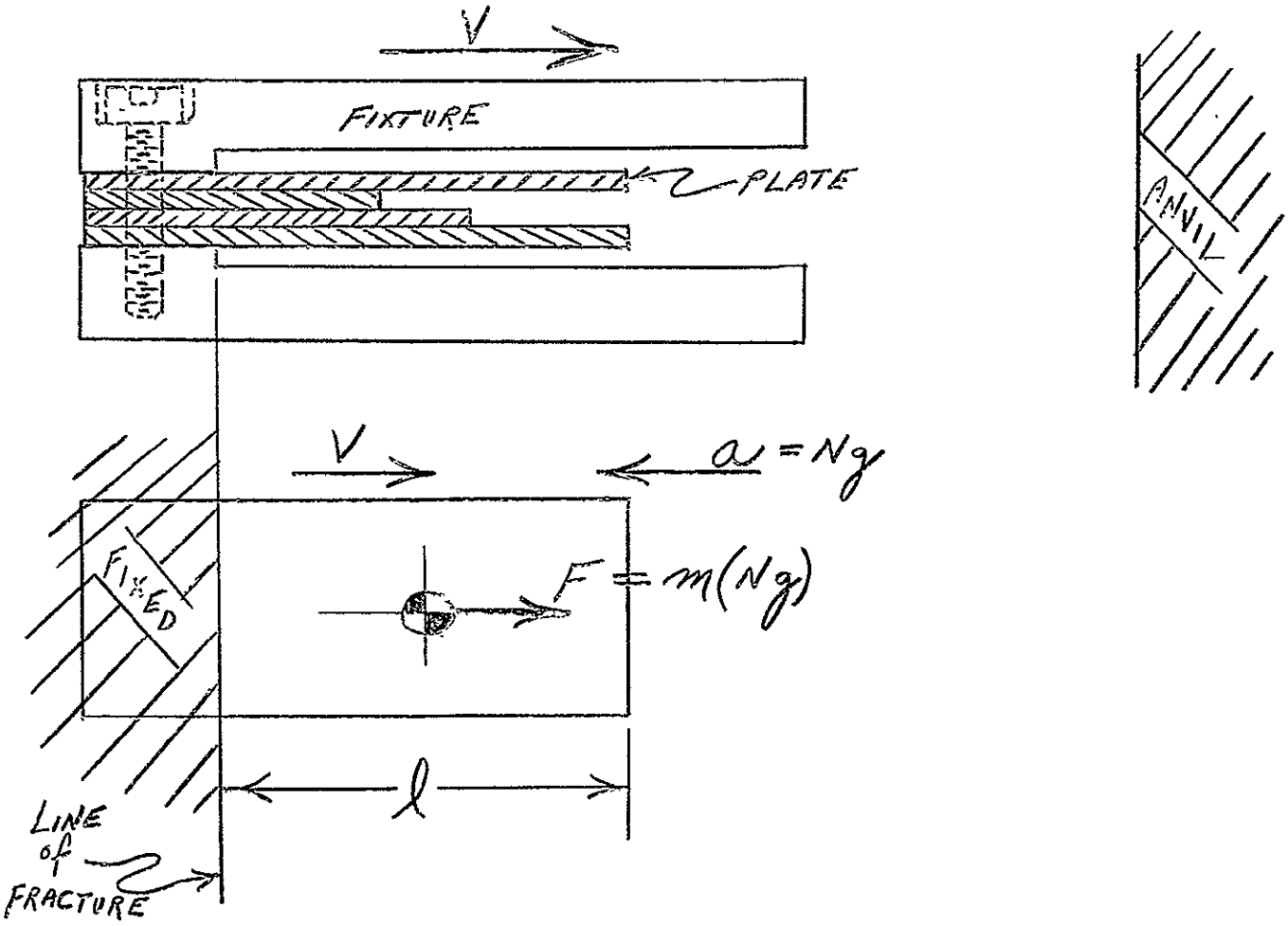

All specimens of positive and negative plate material were constant width (2" or 40 wires) and cut to various lengths (3-1/2" - 6-1/4"). Typically, four positive plates and four negative plates, each of a different length, would be

placed in the fixture. Through suitable shims, friction elimination techniques, and clamping arrangements, we could consider one end fixed. Then, knowing the effective free length, l, the mass density, ρ, and the mean g-level at impact, Ng, we could calculate for each plate the dynamic tensile inertia force experienced. Therefore, lengths were varied above and below the predetermined static failure length. The results of this type of dynamic testing are best shown in Fig. III-D. Each line on this one-dimensional plot represents a given plate which has experienced impact and has either failed or resisted the tensile loading imposed. Experimental effects are responsible for some overlap but the density of lines indicates an approximate value of dynamic ultimate load. These values are tabulated below for comparison.

TABLE III- 6

ULTIMATE TENSILE STRENGTH (2" WIDTH)
(As-manufactured Electrodes)

	Static $\dot{\epsilon}$ = Constant	Static $\dot{\sigma}$ = Constant	Dynamic 7/8" Tool	Dynamic 1" Tool
Positive Plate	72#	76#	80#	107#
Negative Plate	76#	79#	90#	115#

What is apparent from this study is that the plate material can support greater loads under dynamic conditions and we indeed may use static strength determinations as a foundation or lower bound for design. In other words, the material is $\dot{\epsilon}$ sensitive

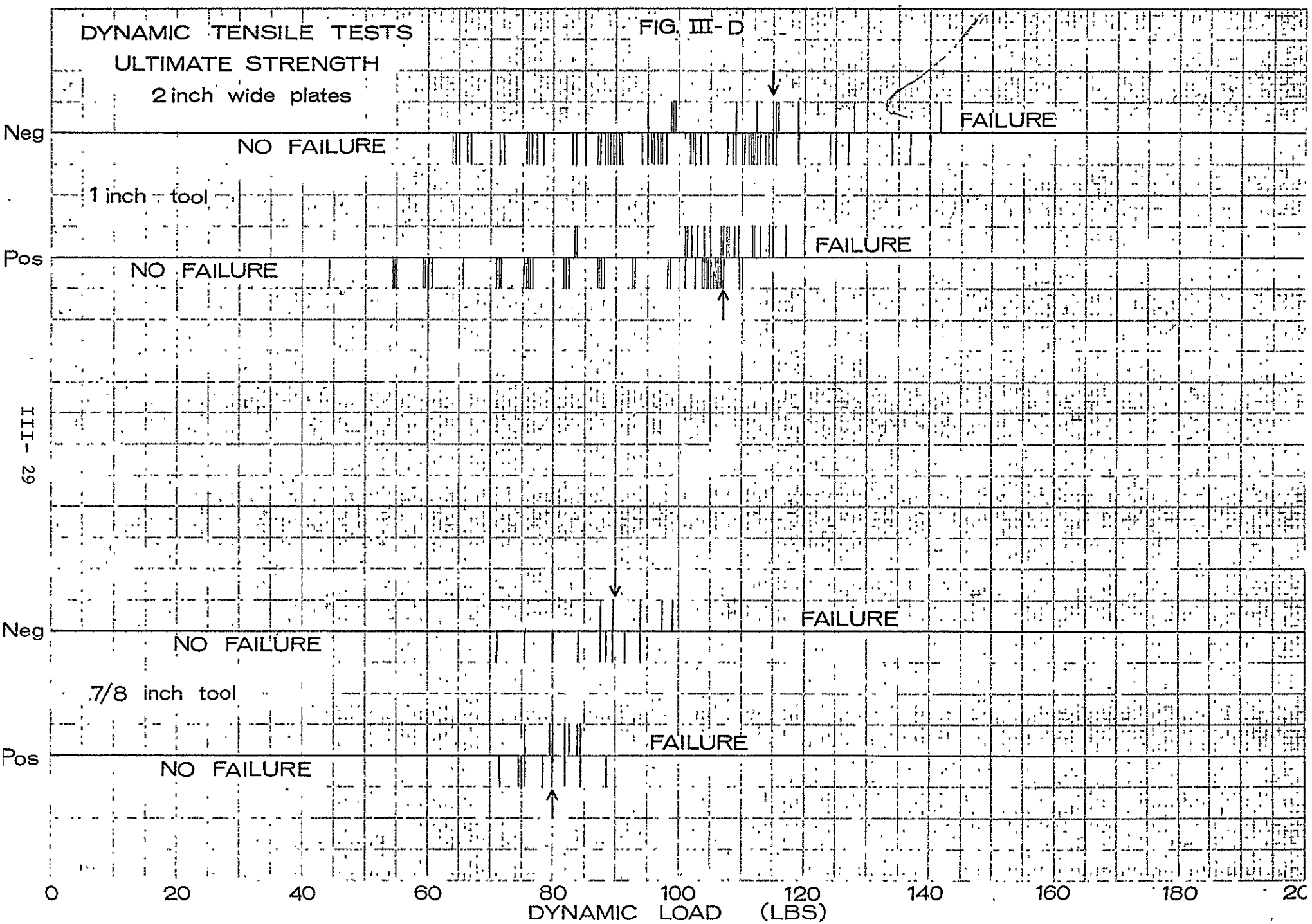
DYNAMIC TENSILE TESTS
ULTIMATE STRENGTH
2 inch wide plates
FIG. III-D
Neg
NO FAILURE
FAILURE
1 inch - tool
Pos
NO FAILURE
FAILURE
Neg
NO FAILURE
FAILURE
7/8 inch tool
Pos
NO FAILURE
FAILURE
0
20
40
60
80
100
120
140
160
180
200
DYNAMIC LOAD (LBS)

and under dynamic loading may support perhaps 120#. The reason that the dynamic tests as reported above are separated is due to the different pulse lengths involved. The calculated values shown are magnified to some degree by the dynamic loading. It is felt that we may indeed be in an area where the magnification is not constant and is dependent upon the natural and applied frequencies involved. This aspect will be discussed in a later report and is not appropriate for this progress report, which intends to merely document the experimental findings to date.

(2) Yield Strength

In addition to bracketing the value of ultimate strength under dynamic loading, we are also able to determine the material's dynamic yield strength, as indicated by the onset of matrix cracking. For example, after impact loading a plate has the appearance shown in the following sketch and in Figure III-E.

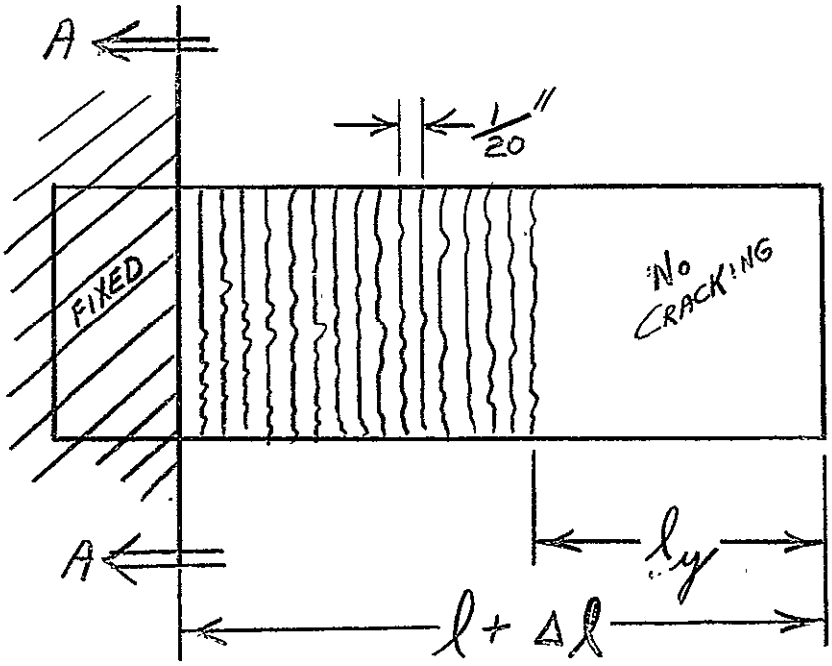

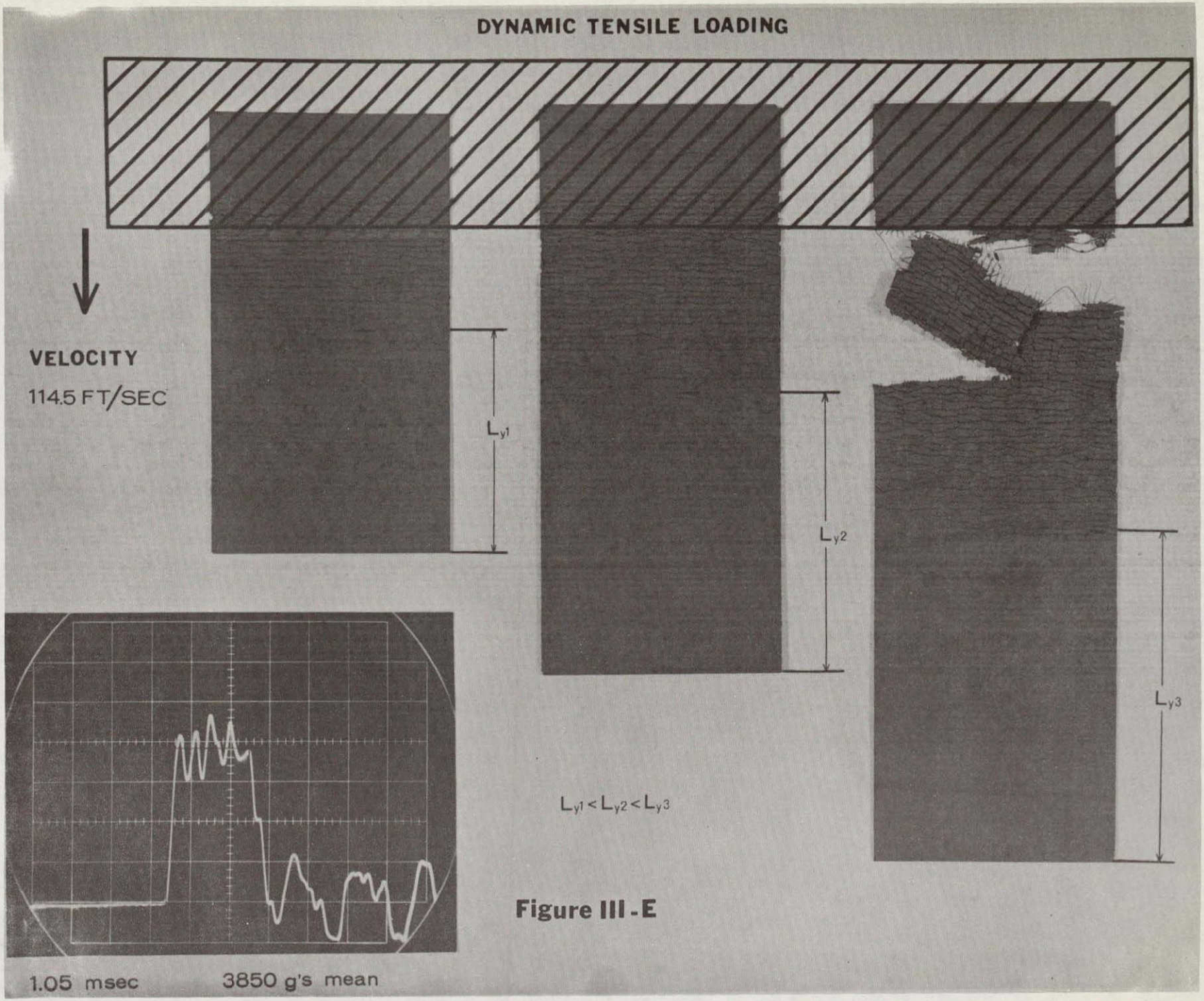
DYNAMIC TENSILE LOADING
VELOCITY
114.5 FT/SEC
L_{y1}
L_{y2}
L_{y3}
$L_{y1} < L_{y2} < L_{y3}$
1.05 msec
3850 g's mean

Figure III-E

As stated previously, the value of effective length, l, will determine whether or not there is sufficient mass experiencing the test acceleration to product a force sufficient to fracture the plate at section A-A. There also exists for each plate a length, l_y, from the free end over which no matrix cracking occurs. Beyond l_y the matrix will have cracks uniformly spaced, each 1/20 inch (20 mesh screen). If we measure l_y for each plate, then, knowing the input acceleration and the physical properties of the plate, we can calculate the dynamic force created by this mass which was responsible for yielding the plate or cracking the matrix. This dynamic yield strength has been calculated for each plate tested and is best shown in Figs. III-F and III-G. We have plotted the yield force, P_y, against the effective plate length, l, since we suspected a distinct function to exist, based on the relative frequency - magnification considerations mentioned. Of course the effect shown is amplified by our failure to consider the progressive nature of yielding. Remaining within the scope of this report, however, we wish only to tabulate the experimental determinations of yield strength that have been accomplished.

TABLE III-7

YIELD STRENGTH (2" WIDTH) (AS-MANUFACTURED ELECTRODES)

	Static $\dot{\epsilon}$ = Constant P_y @ 0.2% ϵ	Static $\dot{\sigma}$ = Constant P_y @ 0.2% ϵ	Dynamic 7/8" Tool P_y @ Crack	Dynamic 1" Tool P_y @ Crack
Positive Plate	44#	45#	60-72#	42-96#
Negative Plate	40#	40#	60-70#	48-78#

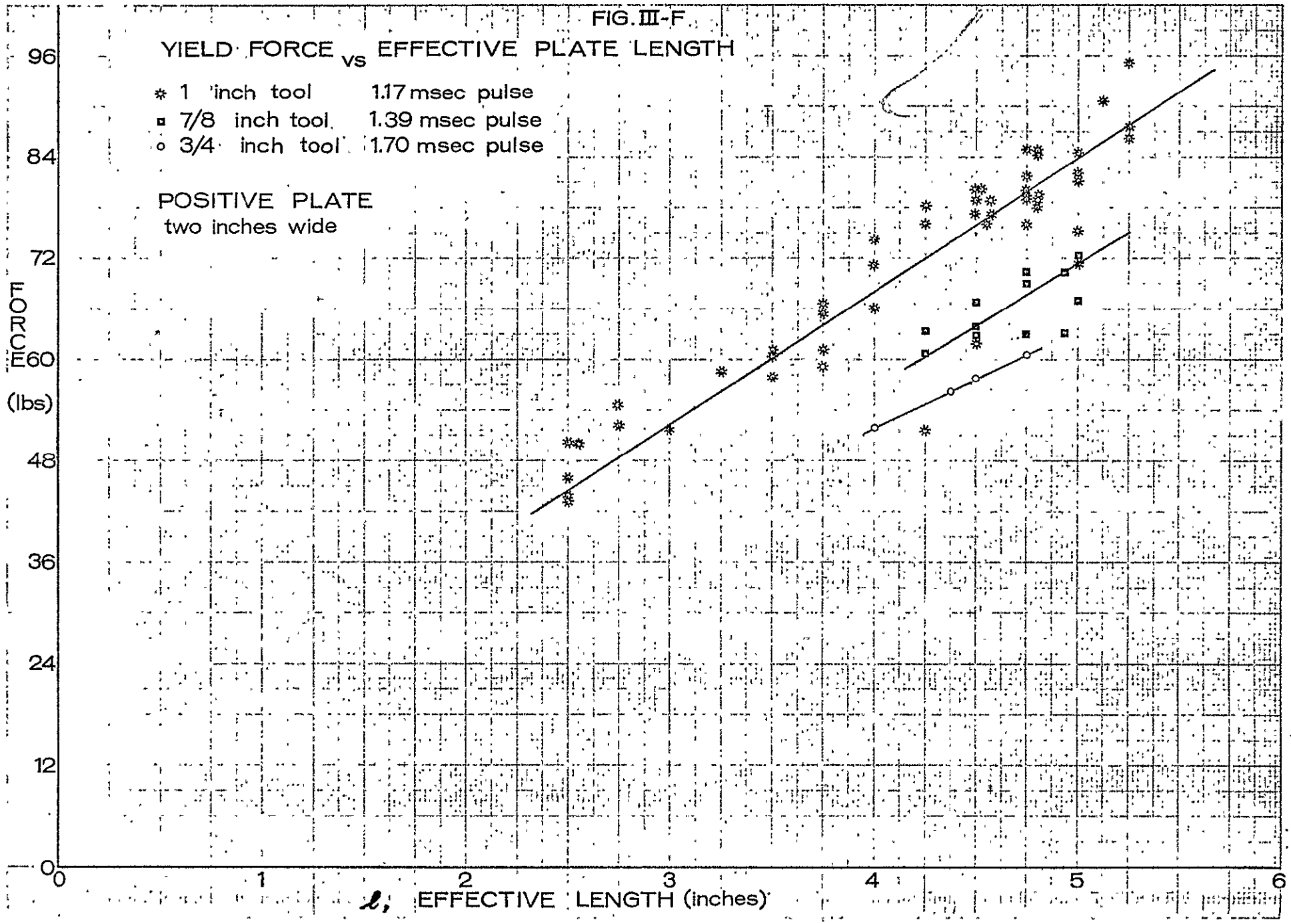
FIG. III-F
YIELD FORCE vs EFFECTIVE PLATE LENGTH
* 1 inch tool 1.17 msec pulse
▫ 7/8 inch tool 1.39 msec pulse
○ 3/4 inch tool 1.70 msec pulse
POSITIVE PLATE
two inches wide
FORCE (lbs)
96
84
72
60
48
36
24
12
0
0
1
2
3
4
5
6
ℓ, EFFECTIVE LENGTH (inches)

Figure III-F

Figure III-G

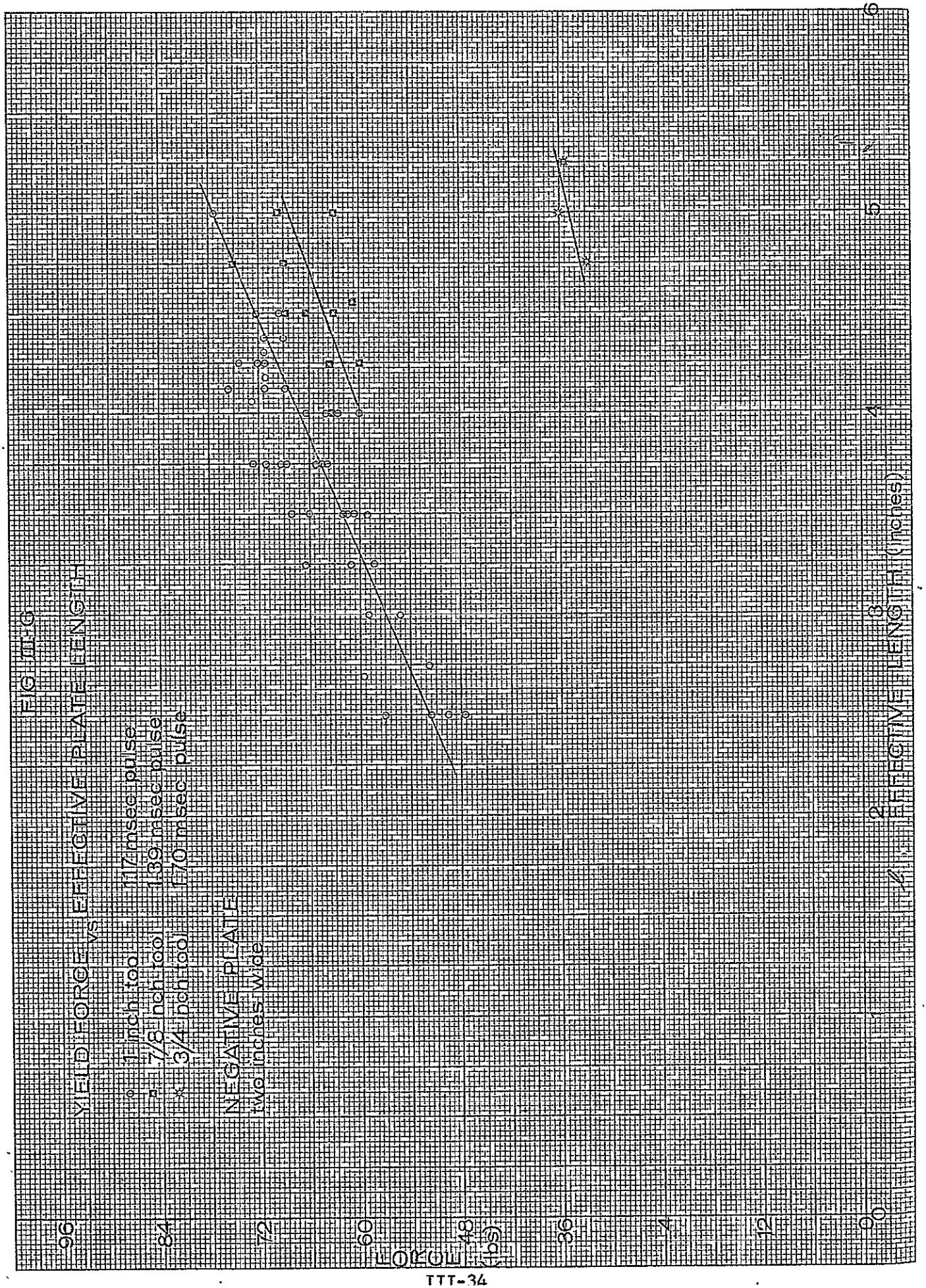
FIG III-G
YIELD FORCE vs EFFECTIVE PLATE LENGTH
1 inch to 7/8 inch top 1.17 msec pulse
3/4 inch top 1.39 msec pulse
NEGATIVE PLATE
two inches wide
FORCE (lbs)
96
84
72
60
48
36
24
12
0
1
2
3
4
5
6
EFFECTIVE LENGTH (inches)

Again, it is apparent that yield strength as well as ultimate strength is elevated by the higher strain rate associated with dynamic loading. The variation with pulse length (7/8" vs 1" tool) and effective plate length must be subsequently considered in detail. For purposes of this report, however, it is only necessary to conclude with the statement that rather complete static stress-strain curves have been established and the effect of strain-rate sensitivity has been shown:

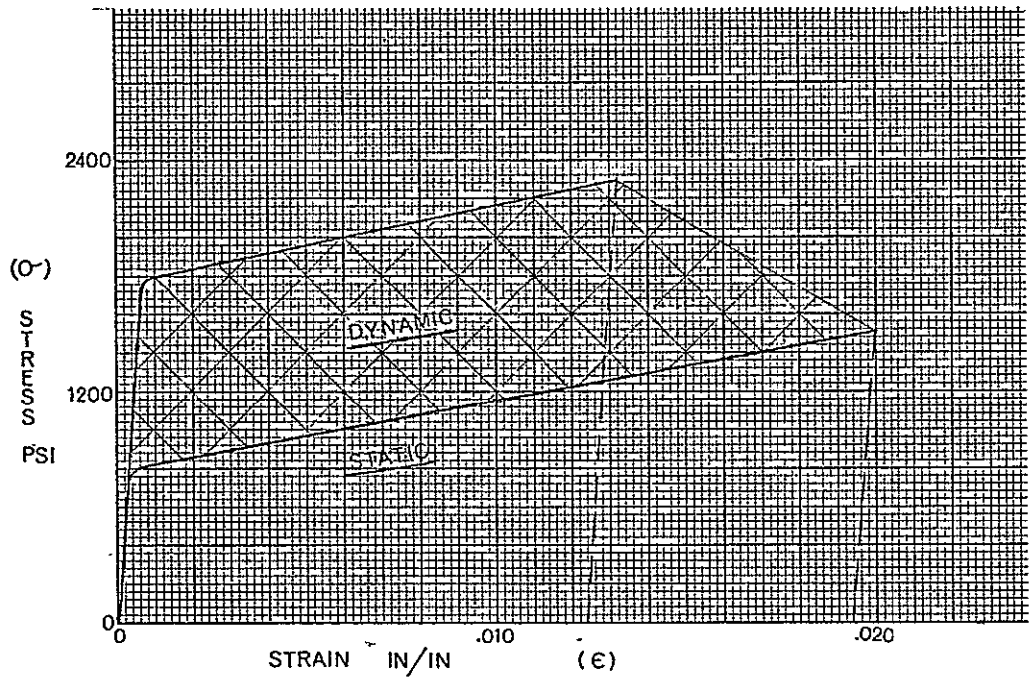

Dynamic strength behavior is elevated above that of the well-established static lower bound. However, the degree of this elevation (shaded area above) is believed to depend on a more well-defined relation between element response and the applied forcing function.

2. MECHANICAL PROPERTIES IN COMPRESSION LOADING

a. INTRODUCTION:

The experimental program for evaluating the mechanical strength of Ni-Cd electrodes may be broadly separated into three (3) distinct methods of loading: tensile, compression, bearing. The behavior under tensile loading has been discussed in section D. 1. The studies of bearing strength are of prime design interest and will be discussed in a subsequent report. It is the scope of this report to describe the manner of loading and the strengths that have been measured in a compression-buckling mode of failure. This area of investigation is similar to the tensile work in that it has primarily increased our understanding of our plates' behavior under load. In contrast, the bearing strength studies will be more clearly related to actual cell failure mechanisms. In other words, edge crushing of the electrode pack may be a prime cell failure mode under impact loading. However, if the plate spacing is significant we may be concerned with compressional buckling behavior and this area will be considered through subsequent work and the information that is contained in this report.

b. CONSTANT DEFORMATION STATIC TESTING:

The static compression loading was accomplished by the constant deformation method (commercial testing machine) as fully described in the tensile report. The manner of specimen loading is shown below:

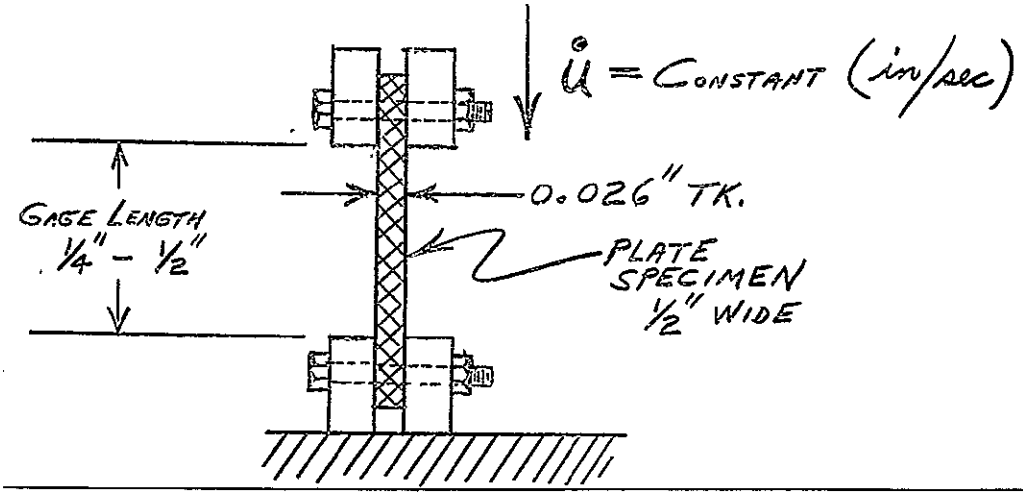

With adequate clamp force, the specimen grips provided a fixed end condition for the plate. The initial gage length was accurately set and the constant machine head speed then provided a strain rate $\dot{\varepsilon} \approx 0.0003\ sec^{-1}$. Two prime failure modes were observed, during the course of our investigation:

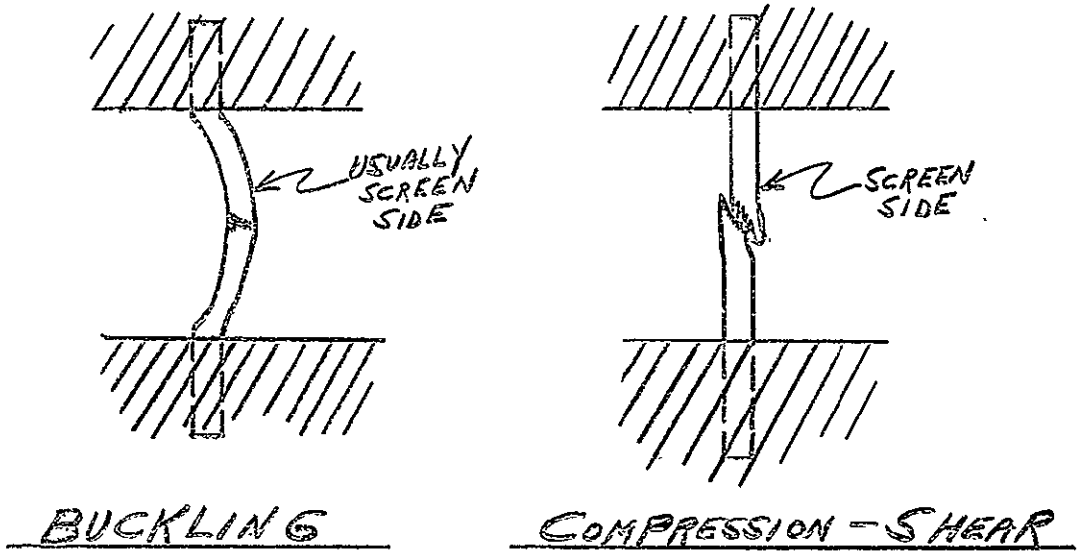

Since the loading system did not provide lateral support, buckling would occur whenever the effective column length was too large for the material strength available. If the material has sufficient strength, buckling is resisted and the higher compressional ultimate load is exhibited.

In the first series of tests, as-manufactured positive and negative electrodes 1/2" wide were loaded over a 1/2" initial gage length. In all cases, the buckling mode of failure was exhibited.

The second series of tests were performed on 1/2" wide specimens of positive and negative plaque over a 1/4" gage length. Again, the universal failure mode was in buckling.

The third series of tests involved as-manufactured positive and negative plates 1/2" wide loaded over a 1/4" gage length. This

was a sufficiently short gage length to permit the specimens to resist buckling and primarily exhibit compressional shear failure.

Reproduceability of stress-strain information for various specimens of the same material is poor when obtained by this manner of loading. Figure III-H presents therefore, average stress-strain curves for the three series of tests. The positive (both plate and plaque) is shown to be stronger than the negative in all cases. The very large increase of plate strength over that of plaque is shown. The large amount of deformation that takes place under very low stress levels is also apparent. Once reinforcement begins at the high strain level it is exhibited by the second modulus designated E_2 which can be seen to be very close to the initial modulus E_1 before yield. Of great significance are the absolute stresses shown in this figure. Regardless of mode of buckling - compressional failure, we observe ultimate stresses of 3000-6000 psi as compared to 1400 psi tensile ultimate stress. It is important that we again indicate that these are average curves indicating the behavior observed and not adequate descriptions of the true compressional strength of our plate structure. It is obvious these are pictures of essentially plastic response to load and we might observe much different behavior if the gage length were 1/8 inch. What may be needed for true compressional evaluation, however, is a measure of the uniform strain over the longer gage length (1/2 inch) with a provision for positive lateral restraint. This approaches the area of bearing strength, however, and will be examined later.

Table III-8 compares the experimental values obtained with some fundamental buckling calculations. E_1 represents the initial apparent modulus of elasticity if significantly exhibited before yield. Following the plastic elongation region, the final "apparent modulus of elasticity" displayed during ultimate loading is represented by E_2. The actual failure load P, is next given but

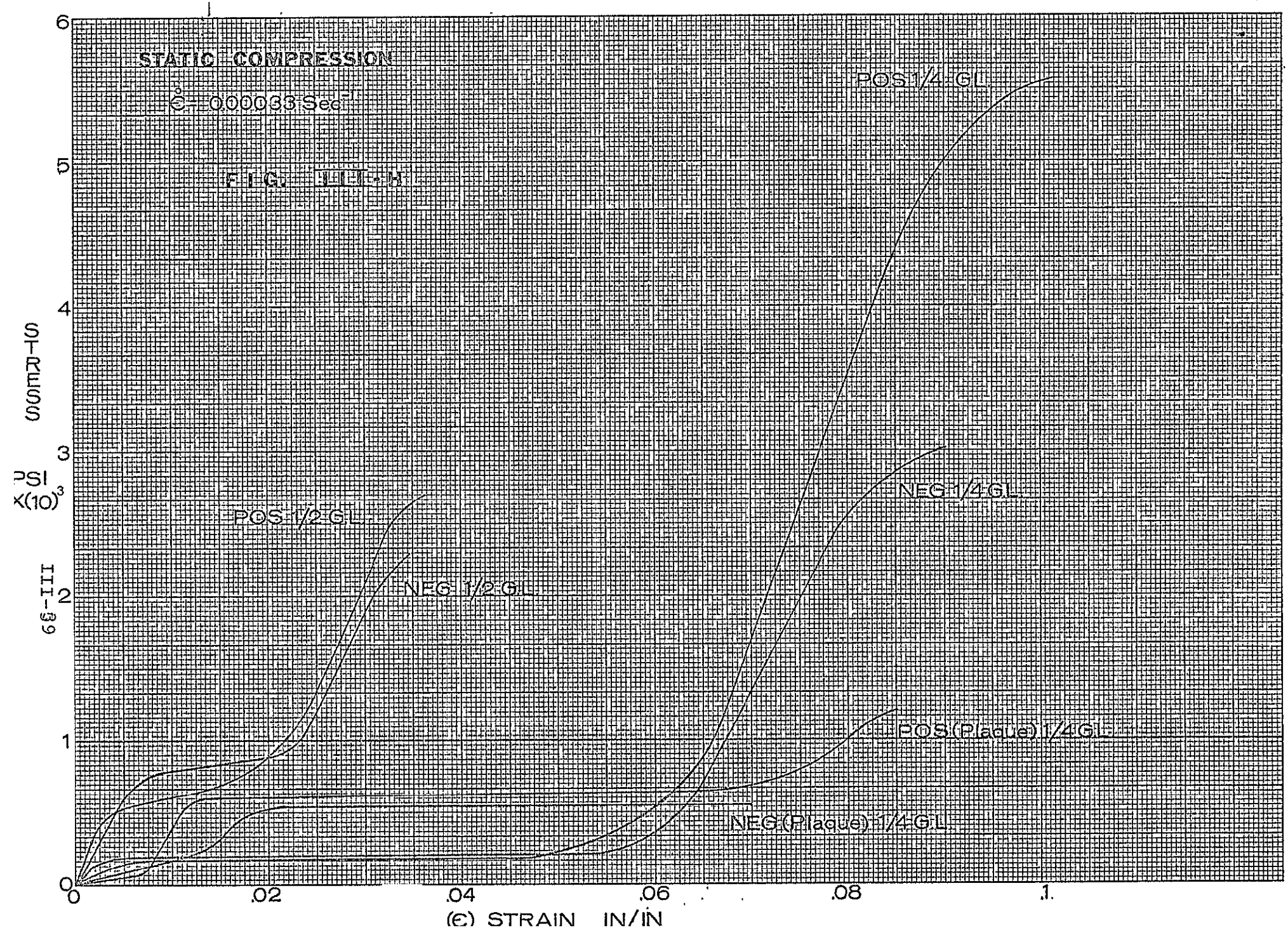
STATIC COMPRESSION
$\dot{\epsilon}$ = 0.00033 Sec^{-1}
FIG. III-H
POS 1/4 GL
NEG 1/4 GL
POS 1/2 GL
NEG 1/2 GL
POS (Plaque) 1/4 GL
NEG (Plaque) 1/4 GL
STRESS PSI X(10)^3
(ε) STRAIN IN/IN
0
1
2
3
4
5
6
.02
.04
.06
.08
.1

TABLE III-8

		E_1 x 10^6 psi	E_2 x 10^6 psi	Static (P) Critical Buckling #	Static (P) Ultimate Compression #	Calculated (P) Critical Buckling $2\left(\frac{\pi^2 E_2 I}{l^2}\right)$	Dynamic (P) Ultimate Compression #
Positive Plate	1/2"	0.24	0.12	35	----	8	
Negative Plate	G.L.	0.12	0.12	32	----	8	
Positive Plaque	1/4"	0.14	0.05	15	----	12	
Negative Plaque	G.L.	----	0.10	8	----	24	
Positive Plate	1/4"	0.14	0.18	---	70	42	>34
Negative Plate	G.L.	0.16	0.16	---	42	36	34

distinguished by the associated mode of failure. Next we have shown a predicted buckling load as calculated by the Euler equation. However, there are several troublesome factors here. The slenderness ratio $(l/r) = (l/\sqrt{I/A})$ in our case is 66 or 33 depending on gage length, and this indicates that we may be out of the Euler region and into an inelastic area better described by the tangent modulus. For this reason we have used the value of E_2 recognizing a strong plastic component yet knowing it remains high for an accurate description of the ultimate load region. Based on experimental observations, we have also compromised with the factor of 4 normally associated with a fixed end condition and treated the specimen as semi-hinged. With such assumptions, the value calculated can be seen to serve merely as a very inaccurate lower limit for comparison purposes. Obviously, a more accurate picture of isolated σ-ε compressional behavior is necessary to improve upon our buckling predictions.

The absolute values of E_2 noted in this type of testing are lower than those observed during constant deformation tensile testing. It also appears from this study, that a rather large amount of plastic deformation is necessary before the matrix is able to support the load. Such factors suggest that the initial bends in the screen wires play a very significant role.

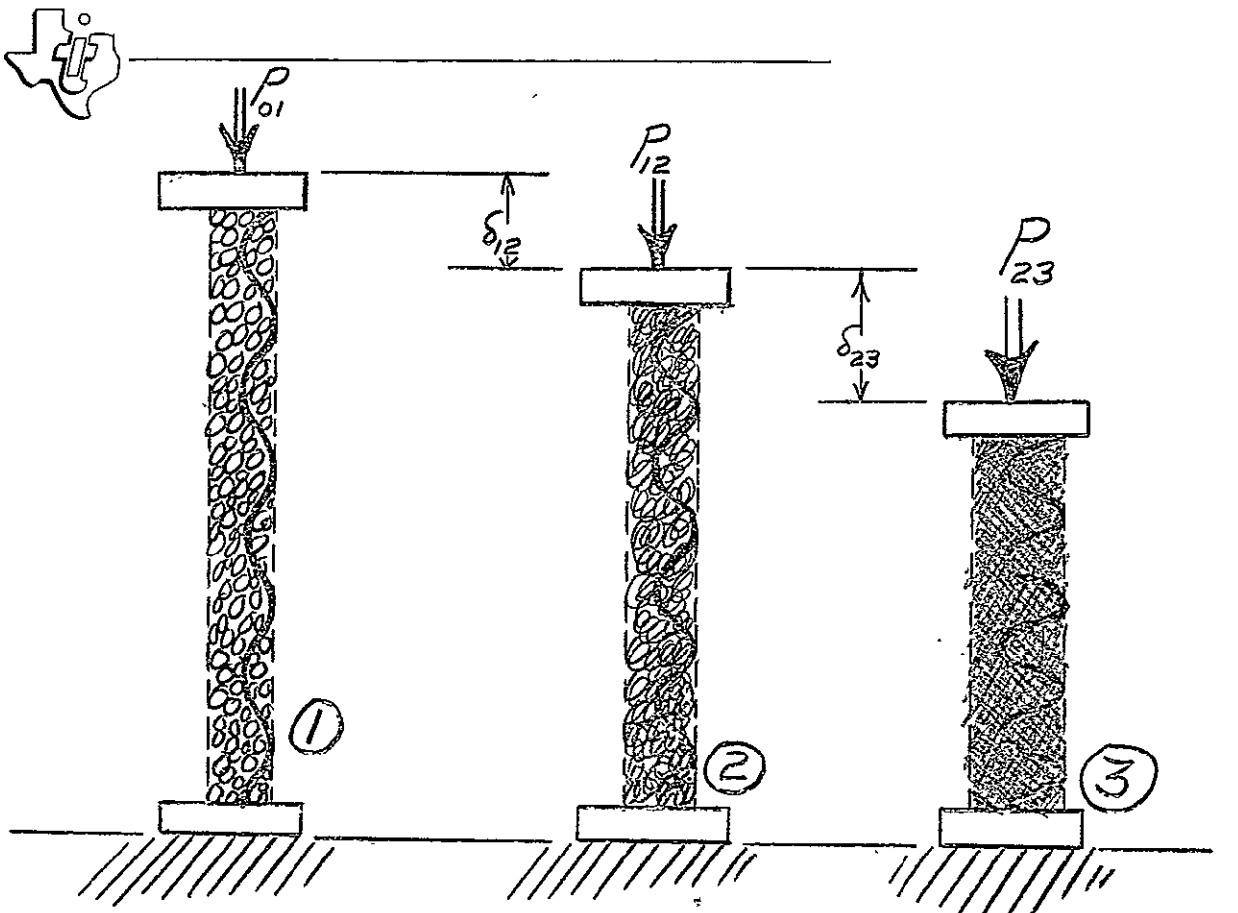

Porous structure uncrushed. Supporting initial load as in tension.

Porous structure has reached yield. Pores collapsing, wire bending.

Sufficient deformation & densification of collapsed pore structure to permit further load support.

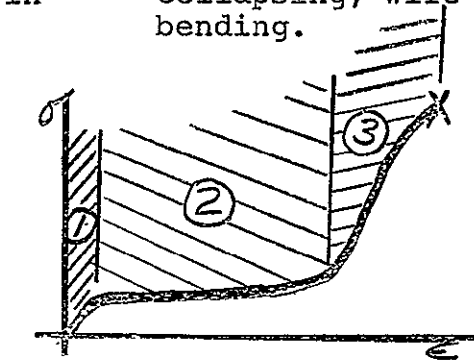

This understanding or explanation is supported by several experimental results. Yield strengths on the order of 100-600 psi have been observed in compression which are lower than those (225-850 psi) experienced under tensile loading. The extensive plastic elongation region is then fairly well established. The modulus E_2 observed when load is again supported is $\leq$ the modulus of screen alone under tensile loading. This indicates that the contribution of screen under compression is reduced and that indeed

from a modulus standpoint, the combination of corrugated screen and compressed sinter are scarcely equal to the screen alone in tension. The ultimate load carrying ability in tension was seen to rely primarily on screen alone since the matrix became ineffective or lost due to elongation. In contrast however, compression appears to utilize the matrix as the major load bearing element up to the point of fracture.

c. DYNAMIC COMPRESSION LOADING

The dynamic test method used to evaluate Ni-Cd plates has been completely described in the tensile loading section D. 1 d. The method used for compression studies is identical except for a reversed mounting procedure which simply allows the plates to experience decelerating forces in the opposite direction.

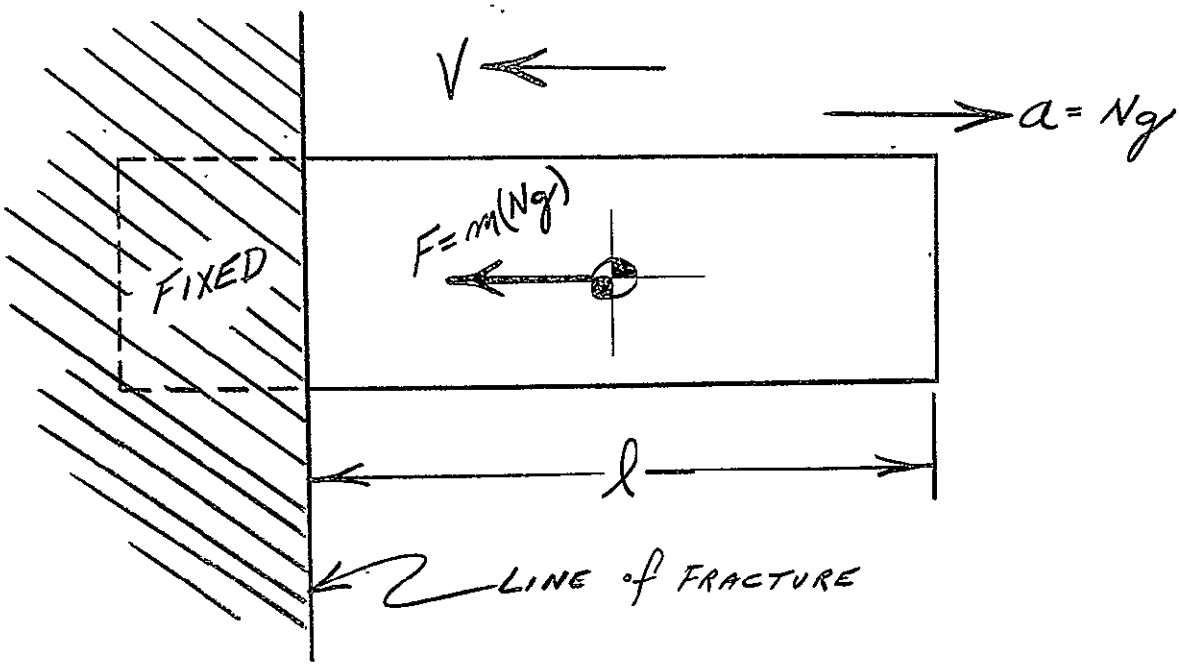

As in tension testing, the compressive specimens were 2" wide and cut to provide various effective lengths, l, for each impact. Through the use of suitable clamping and friction elimination techniques, each plate was essentially free to exhibit its response to the input force. A buckling mode of failure was not permitted, and thus we observed only compresional fracture as shown in Fig. III-I.

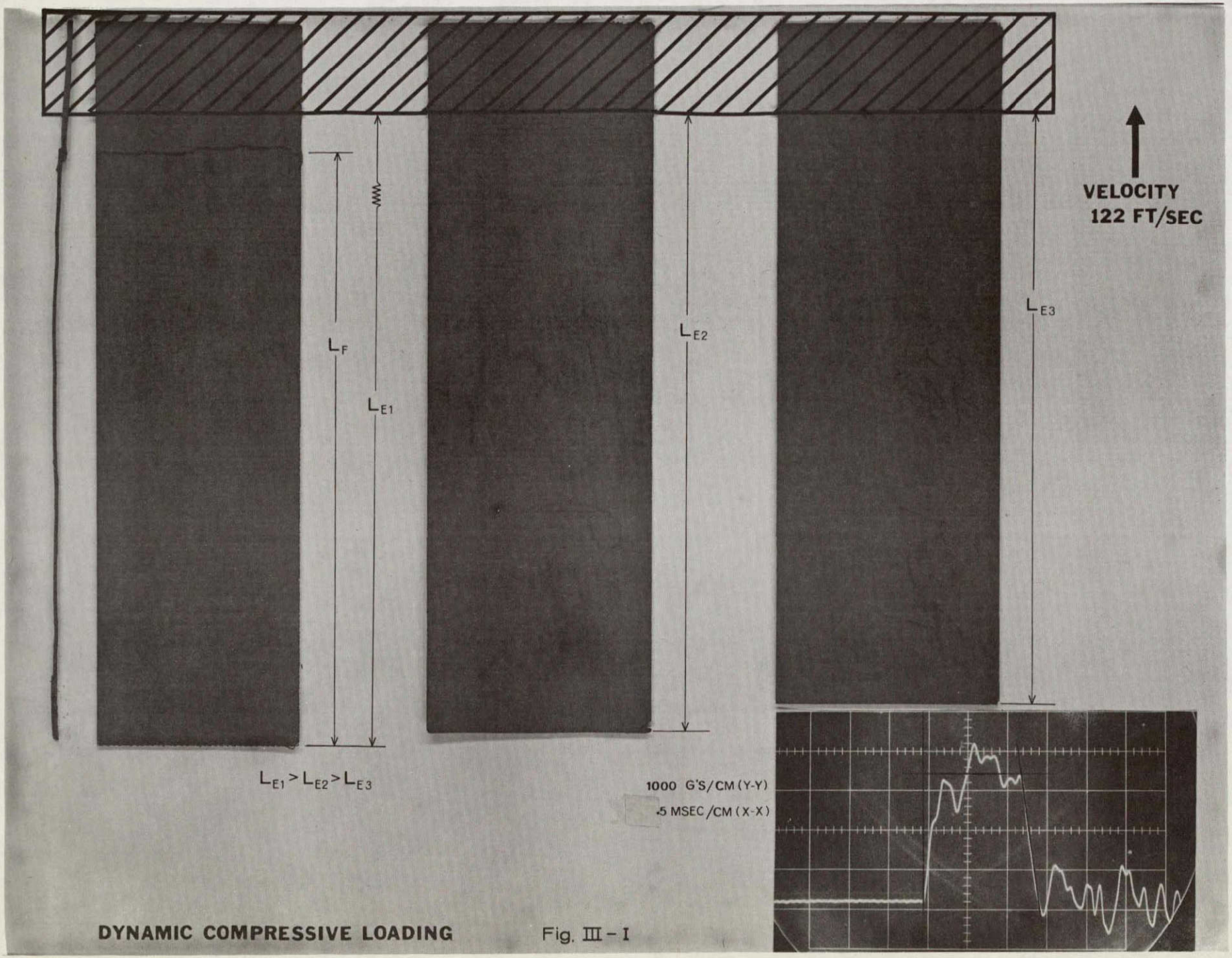

DYNAMIC COMPRESSIVE LOADING Fig. III - I

If the effective length, l, was sufficiently large, failure would occur at the associated loading. A dynamic yield point is not observed in the compression loading of the matrix as was seen in tensile loading. Thus we have merely a determination of the ultimate compression load. Figure III-J displays our results to date. Each line on this one-dimensional plot represents a plate of a given length (effective mass) which experienced a resultant force when subjected to the measured impact deceleration.

Positive Plate has not failed in a completely dynamic compressional mode thus far in our testing. We have observed plates of the maximum effective length permissible (l = 5-7/16") experiencing impact levels of 3700g with no apparent damage in pure dynamic compression. Thus, we may only say at this time that the P_{ult} > 134# or σ_{ult} > 2600 psi. Indications are then, that the positive is stronger than the negative which is in agreement with the very obvious result of static testing.

Negative Plate material has been found to have a fracture load of 135 lbs. for the 2" width (2400 psi). This is slightly lower than the average value obtained in static testing (recall 168 lbs. or 3000 psi). Even recognizing that the static data contained a great deal of scatter, we may assume that some dynamic phenomena are being observed. If our deformation model for compression is valid, it would imply that the Ni metal screen wires are not available at ultimate load to carry significant stress and therefore the strain rate, $\dot{\varepsilon}$, effects observed in tensile loading will not appear in compression. In other words elevation of σ_{ult} in tension at elevated $\dot{\varepsilon}$ was an observable and reasonable effect but we now have reason to expect very little difference in compressional σ_{ult} as a function of $\dot{\varepsilon}$. We do not observe a measurable yield point in our dynamic compression studies and therefore cannot discuss its possible relation to static results. The scope of this report

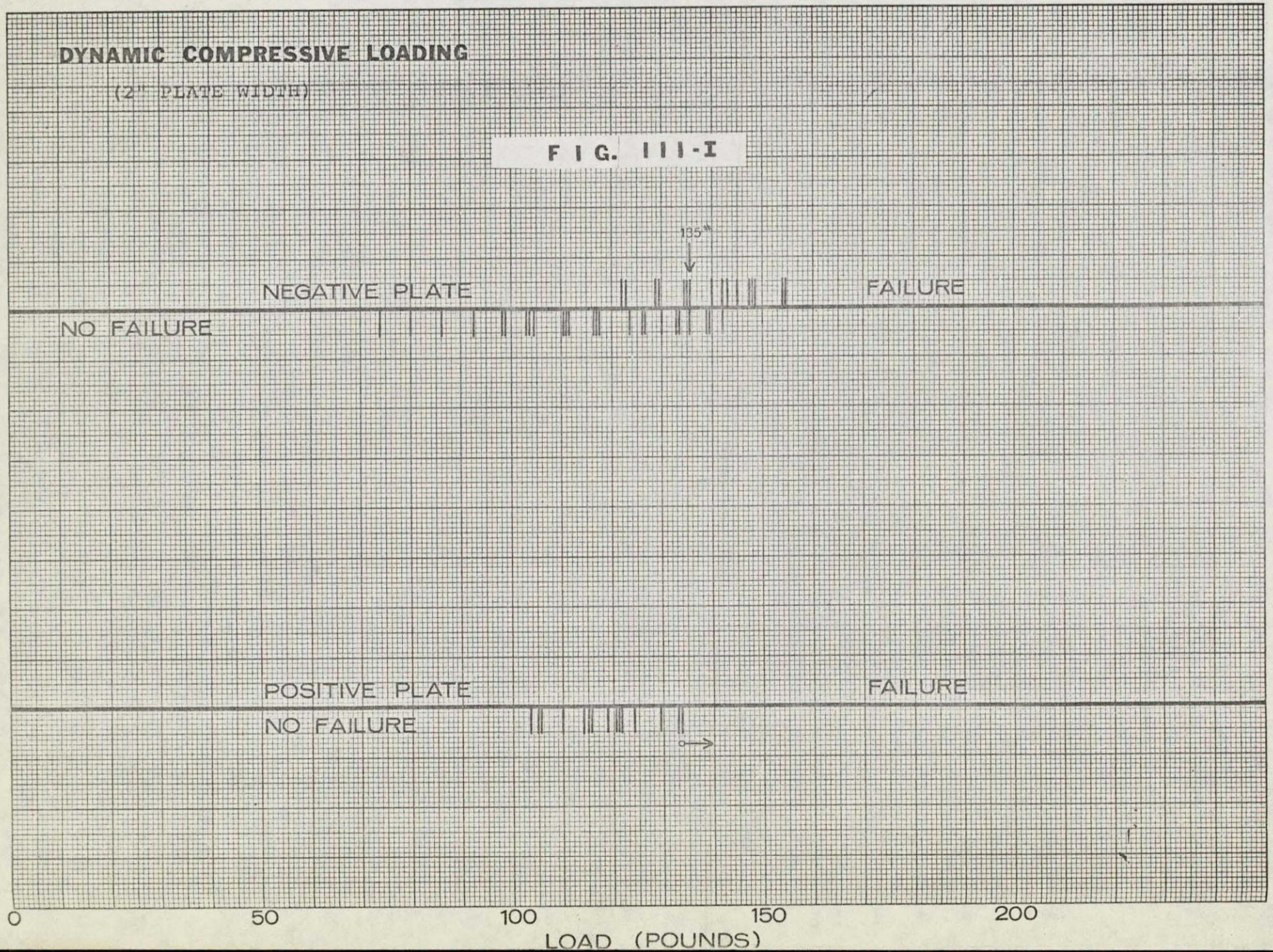

remains however, to present experimental findings to date and to indicate the underlying phenomena that may be responsible. The latter must be subsequently discussed as an entity, however, when all aspects of progressive deformation, natural frequency and forcing function have been considered.

3. EVALUATION OF STRAIN-GAGE TECHNIQUES

During the initial experimental work to determine the stress-strain relation for Ni-Cd electrodes, it was desirable to evaluate the applicability of strain gages for this material. The use of bonded resistance gages to such a porous sintered structure is not common practice and the obvious problems are associated with the surface roughness, porosity, averaging strain and minimizing reinforcement. As in work with aggregate concrete, we must be careful to use a sufficiently large gage length to average strain over discrete pores and screen wires. Ideally the strain gage and cement should not strengthen the structure which is being measured to any appreciable degree. Despite these obvious difficulties, this technique offers the possibility of providing information that would be extremely difficult to measure by any other method. The determination of Poisson's Ratio, the measurement of vibration and damping capacity, the measurement of dynamic strains within a cell, are conceivable and thought to be valid reason for developing a suitable technique.

a. TECHNIQUE DEVELOPMENT

The preliminary investigation involved bonding two types of foil strain gages (epoxy backing 1/2" G.L.) to tensile specimens of positive plate material and loading with dead weights. The linearity of response during loading and unloading in the assumed elastic region, along with some indication of early plastic behavior were encouraging.

Values of the apparent Young's modulus (E_{app}) were found to be 0.65×10^6 psi and 1.97×10^6 psi which were in the range predicted by our analytical model. In addition a value of Poisson's Ratio was obtained of 0.386. These two specimens are shown in Figure III-K (1) and it was obvious that significant reinforcement

Figure III-K

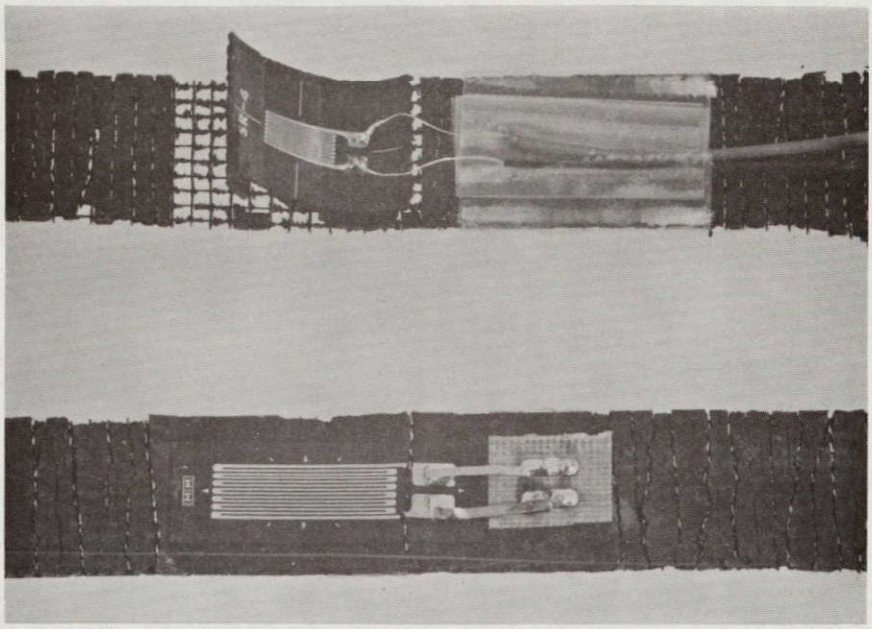

(1)

EPOXY
FOIL
GAGES

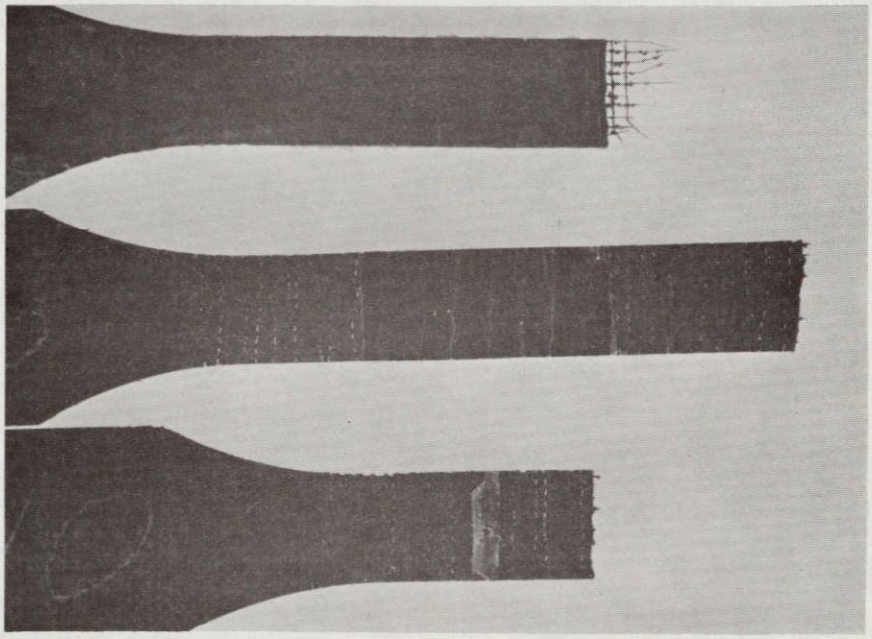

(2)

EPY
150

DUCO

910

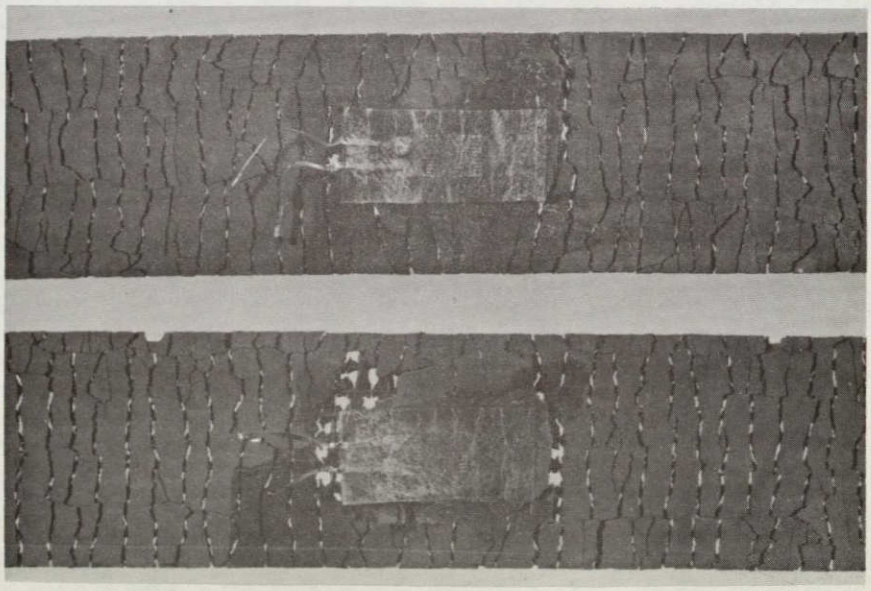

(3)

THIN
PAPER
GAGES

existed. Failure of one gage is noted where a finite matrix crack occured within an essentially infitesimal section of the gage length. In the other case, the gage and cement combination were of sufficient strength to cause a mode of eccentric bending and separation of sinter from the screen.

At this point, several commonly used strain gage cements were evaluated for their compatability and reinforcement. Figure III-K (2) shows three of the most significant studies:

EPY-150: is an epoxy cement commonly used with epoxy foil gages and it was found to offer a great deal of reinforcement. Matrix cracking was almost non-existant and the ultimate strength of the plate material was raised nearly 140 psi. The implication was that not only this cement was unsatisfactory but the entire class of strain gages with epoxy film backing would also be unsatisfactory.

Duco (Nitrocellulose): is also a commonly used cement with paper backed strain gages which were less likely to reinforce the element being measured.

However, a very low frequency of cracking occurred within the test area of this cement. Indications were that yield strength must be considerably increased by this cement also.

Eastman 910: as shown in Figure III-K (2), this cement appears to crack with the sintered matrix in a very uniform fashion. It is compatible with the thin paper backing used in some foil gages and because of its fast-drying behavior, seems to give a minimum of reinforcement when applied to our porous surface.

Two specimens of negative plate material were equipped with one axial strain gage (1/8" G.L. thin paper backed foil type FAP) cemented with a mimimum of Eastman 910. During loading, strain readings from the gage were taken and compared to simultaneous readings from a commercial extensometer mounted directly above the strain gage. The reason for this check was to quantitize the optimized technique's ability to record strain accurately. It was found that the value of strain indicated by the strain gage on the first specimen could be related to the true strain as indicated by the extensometer according to:

$$\varepsilon \text{ gage} = \left[(0.795)\varepsilon \text{ ext} - 72\mu\text{in/in}\right] \qquad 0 < \varepsilon \text{ ext} < 650\mu\text{in/in}$$

and for the second specimen tested:

$$\varepsilon \text{ gage} = \left[(0.795)\varepsilon \text{ ext} + 62\mu\text{in/in}\right], \qquad 0 < \varepsilon \text{ ext} < 200\mu\text{in/in}$$

The results then, indicate that the gage's foil grid, paper backing and surface glue line are responsible for a 20% increase in strength. It was encouraging, however, to note that the reinforcement was consistant and thus predictable. The reason for the intercept required (+ or -) is due to initial loading behavior which seems to imply considerable bending or straightening of screen wires before an accurate state of tension could be monitored. Strain bounds were necessary with these equations to mark the departure of linear (ε ext vs. ε gage) behavior because of gage bending and extraneous deformation as shown in Figure III- K (3).

What has been demonstrated in this study, is that a technique has been developed for strain gages which provides an output relatively insensitive to initial loading problems, linear at 0.8 of true strain value (20% reinforcement), and useable through a low and very limited range of strain.

b. POISSON'S RATIO

At this point, we felt the technique was sufficiently developed to allow a meaningful determination of Poisson's Ratio. An axial strain gage and an identical transverse strain gage of the thin paper foil type were installed with Eastmen 910 on each of three ½" wide dry negative plate specimens. Simultaneous strain readings were taken from each gage and a commercial axial extensometer. Essentially, we compared the slope ratio of the transverse to the axial gage output within the region of linear agreement between the axial gage and the axial extensometer. The constant loading as described in section D 1 b was used for these tests. The third specimen was subjected to one unload-reload cycle to show the elastic behavior more clearly.

The results are presented in Table III-9. We have indicated the modulus of elasticity, E, as determined at various strain, ϵ, levels by unload-reload cycles. The values obtained are in good agreement with those previously determined (Table III-4) by this type of loading. We have also given the calculated ratio of strain gage output to that of the extensometer. This value was given earlier as 0.8 and in some instances we have substantially lower values. Next reported, are the values of Poisson's Ratio, which were obtained from each test. The average value is $\nu = 0.184$. However, more weight must be given to the values obtained at the higher $\left(\frac{\epsilon_{AXIAL\ GAGE}}{\epsilon_{AXIAL\ EXTEN.}}\right)$ ratio since this indicates a lower degree of matrix reinforcement. On this basis, the best value of Poisson's ratio is approximately 0.17 and should be used for subsequent calculations. This value is of course much lower than the 0.28 normally observed with pure nickel metal and indicates a large degree of anisotropy. We had previously observed the differences in tensile and compressive strength, and this predicted anisotropic behavior has been confirmed under this uniaxial loading study.

Further development of this technique might look at "post-yield" strain gages (annealed foil grid to permit higher elongation) to further diminish the reinforcement and extend the useable strain range. Other cements or techniques should also be tried if the measurement of high level dynamic strains is the ultimate goal. It must be noted that technique development is facilitated by studies of tensile loading. But the ϵ-level limits reported, are not applicable to compressive loading situations. In fact, we would expect a very substantial increase in the compressional limits. This is very encouraging when considering our goal of monitoring impact-induced compressive deformations of the electrodes within a cell.

TABLE III-9

Negative Plate Specimen ½" wide		E @ ϵ in/in (PSI)	$\left(\frac{\epsilon \text{ axial gage}}{\epsilon \text{ axial extensometer}}\right)$ ϵ-limits μ in/in	$\left(\frac{\epsilon \text{ transverse gage}}{\epsilon \text{axial extensometer}}\right)$ ϵ-limits in/in	Poisson's Ratio ν
5-28		1.22×10^6 @ .0014 1.00×10^6 @ .0038	0.702 (50-300)	0.116 (50-350)	0.164
6-16		1.30×10^6 @ .0044	0.400 (100-600)	0.088 (100-700)	0.218
6-27	Initial loading	------	0.364 (80-600)	0.068 (20-$>$625)	0.186
	Reload @ 0.0012 in/in	1.01×10^6 average @ .0012	0.733 (10-$>$300)	0.124 (40-$>$300)	0.169

TEXAS INSTRUMENTS
INCORPORATED
METALLURGICAL MATERIALS DIVISION
ATTLEBORO, MASSACHUSETTS U.S.A.

5-MMD-19528 2/69